Available online at www.sciencedirect.com
ScienceDirect
Journal of Sound and Vibration 318 (2008) 50–73
JOURNAL OF SOUND AND VIBRATION
www.elsevier.com/locate/jsvi

Scattering and active acoustic control from a submerged piezoelectric-coupled orthotropic hollow cylinder

Seyyed M. Hasheminejad*, M. Rajabi

Acoustics Research Laboratory, Department of Mechanical Engineering, Iran University of Science and Technology, Narmak, Tehran 16844, Iran

Received 25 September 2007; received in revised form 17 March 2008; accepted 7 April 2008
Handling Editor: A.V. Metrikine
Available online 5 June 2008

Abstract

A general exact analysis for three-dimensional scattering of a time-harmonic plane-progressive sound wave obliquely incident upon an arbitrarily thick bilaminated circular hollow cylinder of infinite extent, which is composed of a cylindrically orthotropic axially polarized piezoelectric inner layer perfectly bonded to an orthotropic outer layer, is presented. An approximate laminate model in the context of the so-called state space formulation along with the classical *T*-matrix solution technique involving a system global transfer matrix is employed to solve for the unknown modal scattering and transmission coefficients. Numerical example is given for an air-filled and water-submerged two-layered elasto-piezoelectric hybrid (steel/PZT4) hollow cylinder insonified by an obliquely incident unit-amplitude plane sound wave. Following the acoustic resonance scattering theory (RST), the total form function amplitude together with the associated global scattering, the far-field inherent background, and the resonance scattering coefficients of the *n*th normal mode are computed as a function of dimensionless frequency for selected angles of incidence, piezoelectric layer thickness parameters, and electrical boundary conditions (i.e., open/closed circuit or active). Also, the electrical voltage coefficients required for partial or complete cancellation of the reflected sound field are calculated. Limiting cases are considered and good agreements with the solutions available in the literature are obtained.

1. Introduction

Among the many types of piezoelectric elements, the (solid or hollow) cylindrical elements of various polarizations are widely used as the principal generators and detectors of acoustic power (i.e., resonators, actuators, transducers, or sensors) in a broad range of practical applications in underwater acoustics, industrial macrosonics, non-destructive testing (NDT), medical diagnostics, electro-optics, communications, and geophysical investigations [1–3]. For example, axially polarized piezoelectric hollow cylinders, one of the much popular form of these elements are generally used as a driver in underwater electroacoustic sonar projectors, or as an aligner (a translator) in a scanning tunnelling microscope [4,5]. Here we shall primarily survey the important research works on dynamics of fluid-loaded piezoelectric cylinders and cylindrical shells.

*Corresponding author. Tel.: +98 21 73912936; fax: +98 21 7451143.
E-mail address: hashemi@iust.ac.ir (S.M. Hasheminejad).

0022-460X/$ - see front matter © 2008 Elsevier Ltd. All rights reserved.
doi:10.1016/j.jsv.2008.04.005

Howarth et al. [6] presented an active (non-reflective) acoustic coating, consisting of a pair of piezoelectric polymer sensors and a thickness extensional mode piezocomposite transducer (actuator), to prevent an incident sound wave from reflecting off the acoustic boundary of a submerged object. Shul'ga et al. [7] and Rudnitskii and Shul'ga [8] investigated the sensitivity (directivity) of a cylindrical piezoceramic shell as a sound pressure receiver to its orientation in the sound field. Babaev et al. [9] studied the interaction of an obliquely incident weak external plane shock wave with an infinitely long piezoceramic cylindrical shell, positioned near a plane boundary (a rigid wall or free surface), based on the Kirchhoff–Love thin shell theory. Belova et al. [10] proposed to use a finite-difference scheme constructed by the integro-interpolation method to solve the non-stationary wave problem for an infinitely long hollow piezoelectric ceramic cylinder immersed in a liquid and excited by an electric signal. Vovk and Oliynik [11] used the partial domains method to examin acoustic characteristics of (sound radiation from) a liquid-filled piezoceramic cylindrical shell with an asymmetric internal insertion for different configurations. Glazanov and Mikhailov [12] proposed an approximate method for calculating the acoustic field produced by a finite-height cylindrical piezoceramic transducer with allowance for the radiation from the ends of its inner volume that is filled with an elastic medium characterized by an arbitrary Poisson's ratio. Babaev and Babaev [13] used coupled electroelasticity theory, acoustic approximation, and two-wire transmission line theory to study the generation of waves by a submerged cylindrical piezoelectric transducer connected by a cable to a source of non-stationary electric signals. Zhang et al. [14] employed the theories of Midline plate, piezoelectricity, viscoelastic materials and fluid dynamics to present the finite element modelling of a fluid-filled cylindrical shell with active constrained layer damping. Liu and Lee [15] used the normal-mode expansion method to develop a mathematical model to describe the scattering of a plane wave obliquely incident on a piezoelectric hexagonal 6 mm cylinder in a fluid. The sensitivities of Rayleigh, Whispering Gallery, and guided wave resonances to perturbations in elastic and piezoelectric constants were discussed.

The above review indicates that, while there exists a notable body of literature on dynamics of fluid-loaded piezoelectric cylinders and cylindrical shells, there seems to be no rigorous investigations on acoustic scattering and cancellation of an incident wave field from a cylindrical shell structure (hollow cylinder). The primary purpose of the current work is to fill this gap. Consequently, we adopt the normal-mode expansion method in combination with the classical T-matrix solution approach and novel features of resonance scattering theory (RST) to investigate the scattering and active control of a plane harmonic progressive sound wave obliquely incident upon a bilaminate orthotropic/piezoelectric hollow cylinder based on full equations of piezoelectricity. The proposed model is of interest due to its inherent value as a canonical problem in structural acoustics. It is of practical value for efficient utilization of piezoelectric materials as sensors and actuators in the control of general fluid–structure coupling dynamic problems involving cylindrical shells [16]. It can also be easily extended to a more general configuration with an arbitrarily number of elastic or piezoelectric layers. The presented exact solution can be used as the benchmark for comparison to other solutions obtained by strictly numerical or asymptotic approaches. It can particularly serve as diagnostic or test cases for purely numerical techniques that attempt to combine elastic, piezoelectric, and fluid-loading effects.

2. Formulation

2.1. Acoustic field equations

Consider a time harmonic infinite plane acoustic wave, with the circular frequency ω, obliquely incident at an angle α on a submerged and fluid-filled bilaminate hollow cylinder of infinite length which is composed of an outer layer of orthotropic material and an inner layer of axially polarized piezoelectric material, with a_0 and a_q being the inner and outer radius of the piezoelectric layer, and a_q and a_{q+s} being the inner and outer radius of the orthotropic layer, respectively. The problem geometry is depicted in Fig. 1a, where (x,y,z) is the Cartesian coordinate system with origin at O, the z direction is coincident with the axis of the hollow cylinder, and (r,θ,z) is the corresponding cylindrical polar coordinate system. Following the standard methods of theoretical acoustics, the field equations for an inviscid and ideal compressible medium that cannot support

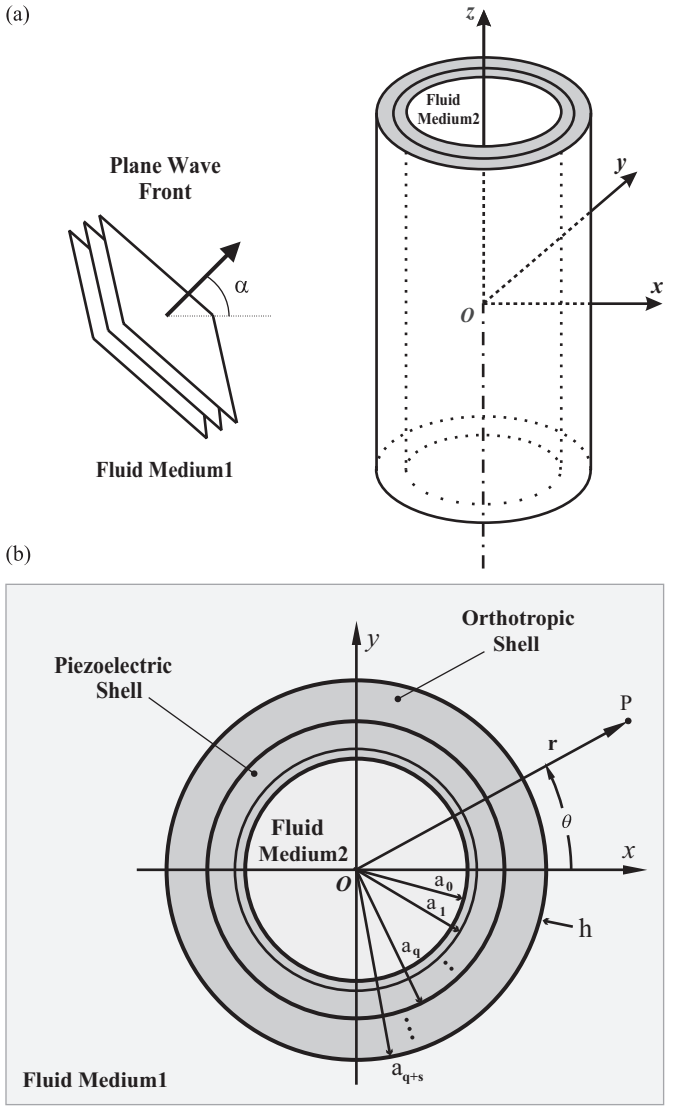

Fig. 1. Problem geometry.

shear stresses may conveniently be expressed in terms of a scalar velocity potential as [17]

$$\mathbf{v} = -\nabla\varphi, \quad p = -\mathrm{i}\omega\rho\varphi, \quad \nabla^2\varphi + k^2\varphi = 0, \tag{1}$$

where $k = \omega/c$ is the wavenumber for the dilatational wave, c is the speed of sound, ρ is the ambient density, $\mathbf{v}$ is the fluid particle velocity vector, and p is the acoustic pressure.

The dynamics of the problem may be expressed in terms of appropriate scalar potentials that can be represented in the form of an infinite generalized Fourier series whose unknown scattering coefficients are to be determined by imposing the proper boundary conditions. The expansion of the incident plane wave, propagating in the surrounding fluid medium, in cylindrical coordinate has the form [18]

$$\varphi_{\mathrm{inc.}}(r,\theta,\omega) = \varphi_0 \sum_{n=0}^{\infty} \varepsilon_n \mathrm{i}^n J_n(k_r r)\cos(n\theta)\,\mathrm{e}^{\mathrm{i}(k_z z-\omega t)}, \tag{2}$$

where $k_z = k\sin\alpha$, $k_r = k\cos\alpha$, $k = \omega/c_1$ is the wavenumber in the outer fluid medium 1 (see Fig. 1a), J_n is the cylindrical Bessel function of the first kind of order n [19], symbol ε_n is the Neumann factor ($\varepsilon_n = 1$ for $n = 0$,

and $\varepsilon_n = 2$ for $n>0$), $\mathrm{i} = \sqrt{-1}$, and φ_0 is the amplitude of the incident wave. Likewise, keeping in mind the radiation condition, the solutions of the Helmholtz equation for the scattered potential in the surrounding fluid medium 1, and the transmitted potential in the inner fluid medium 2 can respectively, be expressed as a linear combination of cylindrical waves as [18]

$$\varphi_1(r,\theta,\omega) = \sum_{n=0}^{\infty} \varepsilon_n \mathrm{i}^n A_n(\omega) H_n^{(1)}(k_r r)\cos(n\theta)\,\mathrm{e}^{\mathrm{i}(k_z z-\omega t)},$$
$$\varphi_2(r,\theta,\omega) = \sum_{n=0}^{\infty} \varepsilon_n \mathrm{i}^n B_n(\omega)\, J_n(K_r r)\cos(n\theta)\,\mathrm{e}^{\mathrm{i}(k_z z-\omega t)}, \tag{3}$$

where $K_r = \sqrt{K^2 - k_z^2}$, $K = \omega/c_2$ is the acoustic wavenumber in the inner medium 2, $H_n^{(1)}(x) = J_n(x) + \mathrm{i}\,Y_n(x)$ is the cylindrical Hankel function of the first kind of order n, $Y_n(x)$ is the cylindrical Bessel function of the second kind of order n [19], and A_n and B_n are unknown scattering/transmission coefficients. Furthermore, using Eq. (1), the acoustic pressures and radial velocities in the fluid mediums 1 and 2 are, respectively, written as

$$\begin{aligned} p_1 &= -\mathrm{i}\omega\rho_1(\varphi_{\mathrm{inc.}} + \varphi_1) \\ &= -\omega\rho_1 \sum_{n=0}^{\infty} \mathrm{i}^{n+1}\varepsilon_n[\varphi_0 J_n(k_r r) + H_n^{(1)}(k_r r)A_n(\omega)]\cos(n\theta)\,\mathrm{e}^{\mathrm{i}(k_z z-\omega t)}, \\ p_2 &= -\mathrm{i}\omega\rho_2\varphi_2 = -\omega\rho_2 \sum_{n=0}^{\infty} \varepsilon_n \mathrm{i}^{n+1} J_n(K_r r)B_n(\omega)\cos(n\theta)\,\mathrm{e}^{\mathrm{i}(k_z z-\omega t)} \end{aligned} \tag{4}$$

and

$$\begin{aligned} v_r^{(1)} &= -\frac{\partial(\varphi_{\mathrm{inc.}} + \varphi_1)}{\partial r} = -k_r \sum_{n=0}^{\infty} \varepsilon_n \mathrm{i}^n \left[\varphi_0 J_n'(k_r r) + H_n^{(1)'}(k_r r)A_n(\omega)\right]\cos(n\theta)\,\mathrm{e}^{\mathrm{i}(k_z z-\omega t)}, \\ v_r^{(2)} &= -\frac{\partial\varphi_2}{\partial r} = -K_r \sum_{n=0}^{\infty} \varepsilon_n \mathrm{i}^n J_n'(K_r r)B_n(\omega)\cos(n\theta)\,\mathrm{e}^{\mathrm{i}(k_z z-\omega t)}, \end{aligned} \tag{5}$$

where prime denotes differentiation with respect to the argument.

2.2. Modal transfer matrix for the orthotropic layer

An orthotropic homogeneous material is characterized by nine independent elastic constants, for which the generalized Hooke's law in the cylindrical coordinate system is written as [20]

$$\begin{Bmatrix} \sigma_{rr} \\ \sigma_{\theta\theta} \\ \sigma_{zz} \\ \sigma_{z\theta} \\ \sigma_{rz} \\ \sigma_{r\theta} \end{Bmatrix} = \begin{bmatrix} c_{11}^o & c_{12}^o & c_{13}^o & 0 & 0 & 0 \\ c_{12}^o & c_{22}^o & c_{23}^o & 0 & 0 & 0 \\ c_{13}^o & c_{23}^o & c_{33}^o & 0 & 0 & 0 \\ 0 & 0 & 0 & c_{44}^o & 0 & 0 \\ 0 & 0 & 0 & 0 & c_{55}^o & 0 \\ 0 & 0 & 0 & 0 & 0 & c_{66}^o \end{bmatrix} \begin{Bmatrix} \gamma_{rr} \\ \gamma_{\theta\theta} \\ \gamma_{zz} \\ 2\gamma_{\theta z} \\ 2\gamma_{rz} \\ 2\gamma_{r\theta} \end{Bmatrix}, \tag{6}$$

where c_{ij}^o are the elastic constants, σ_{ij} and γ_{ij} are the stress and strain components in the orthotropic layer, respectively, and

$$\begin{aligned} &\gamma_{rr} = \frac{\partial u_r}{\partial r}, \quad \gamma_{\theta\theta} = \frac{\partial u_\theta}{r\,\partial\theta} + \frac{u_r}{r}, \quad \gamma_{zz} = \frac{\partial u_z}{\partial z}, \\ &\gamma_{r\theta} = \frac{1}{2}\left(\frac{\partial u_r}{r\,\partial\theta} + \frac{\partial u_\theta}{\partial r} - \frac{u_\theta}{r}\right), \quad \gamma_{\theta z} = \frac{1}{2}\left(\frac{\partial u_z}{r\,\partial\theta} + \frac{\partial u_\theta}{\partial z}\right), \quad \gamma_{rz} = \frac{1}{2}\left(\frac{\partial u_z}{\partial r} + \frac{\partial u_r}{\partial z}\right), \end{aligned} \tag{7}$$

where u_r, u_θ and u_z are the material displacements in the r, θ and z directions, respectively. Also, the equations of motion, in the absence of body forces, in terms of the stress components are written as [21]

$$\frac{\partial\sigma_{rr}}{\partial r}+\frac{\partial\sigma_{r\theta}}{r\,\partial\theta}+\frac{\partial\sigma_{rz}}{\partial z}+\frac{1}{r}(\sigma_{rr}-\sigma_{r\theta})=\rho_o\frac{\partial^2 u_r}{\partial t^2},\quad \frac{\partial\sigma_{r\theta}}{\partial r}+\frac{\partial\sigma_{\theta\theta}}{r\,\partial\theta}+\frac{2}{r}\sigma_{r\theta}+\frac{\partial\sigma_{z\theta}}{\partial z}=\rho_o\frac{\partial^2 u_\theta}{\partial t^2},$$
$$\frac{\partial\sigma_{rz}}{\partial r}+\frac{\partial\sigma_{\theta z}}{r\,\partial\theta}+\frac{\sigma_{rz}}{r}+\frac{\partial\sigma_{zz}}{\partial z}=\rho_o\frac{\partial^2 u_z}{\partial t^2}, \tag{8}$$

where ρ_o is the material density of the orthotropic layer.

Now, following the state space approach [22], the state equation can be readily derived by direct substitution of the constitutive relations (6) and (7) into the equations of motion (8), which after some tedious manipulations, leads to:

$$\frac{\partial\mathbf{Y}^o}{\partial r}=\mathbf{M}^o\mathbf{Y}^o, \tag{9}$$

where $\mathbf{Y}^o=[u_r,\quad u_\theta,\quad u_z,\quad \sigma_{rr},\quad \sigma_{r\theta},\quad \sigma_{rz}]^{\mathrm{T}}$, is the state vector, and $\mathbf{M}^o$ is a 6×6 coefficient matrix whose elements are provided in Appendix A. Next, by employing the appropriate normal mode expansions [22], the state vector $\mathbf{Y}^o$ is expanded in terms of unknown modal coefficients as

$$\mathbf{Y}^o=\begin{Bmatrix}u_r\\ u_\theta\\ u_z\\ \sigma_{rr}\\ \sigma_{r\theta}\\ \sigma_{rz}\end{Bmatrix}=\sum_{n=0}^{\infty}\begin{Bmatrix}\mathrm{a}_{q+s}u_r^n(\eta)\cos(n\theta)\\ \mathrm{a}_{q+s}u_\theta^n(\eta)\sin(n\theta)\\ \mathrm{a}_{q+s}u_z^n(\eta)\cos(n\theta)\\ c_{44}^o\sigma_{rr}^n(\eta)\cos(n\theta)\\ c_{44}^o\sigma_{r\theta}^n(\eta)\sin(n\theta)\\ c_{44}^o\sigma_{rz}^n(\eta)\cos(n\theta)\end{Bmatrix}\mathrm{e}^{\mathrm{i}(k_z z-\omega t)}, \tag{10}$$

where $\eta=r/\mathrm{a}_{q+s}$ is the dimensionless radial coordinate. Subsequent substitution of Eq. (10) into Eq. (9), and utilizing the orthogonality of trigonometric functions, we obtain

$$\frac{\mathrm{d}\mathbf{V}_n^o}{\mathrm{d}\eta}=\mathbf{D}_n^o\mathbf{V}_n^o, \tag{11}$$

where $\mathbf{V}_n^o=[u_r^n,\quad u_\theta^n,\quad u_z^n,\quad \sigma_{rr}^n,\quad \sigma_{r\theta}^n,\quad \sigma_{rz}^n]^{\mathrm{T}}$, is the modal state vector, and $\mathbf{D}_n^o$ is a 6×6 modal coefficient matrix whose elements are given in Appendix A. Direct solution of Eq. (11) is very difficult, as the elements of $\mathbf{D}_n^o$ are not constants (i.e., they are functions of the radial coordinate η; see Appendix A). Hence, by adopting a laminate model [22], the orthotropic cylindrical layer may be assumed to be composed of s sublayers of equal thickness, $h_s=(\mathrm{a}_{q+s}-\mathrm{a}_q)/s$ which are perfectly bonded at their interfaces and lined up such that their axes of symmetry coincide with each other (see Fig. 1b). As the thickness of each sublayer is supposed to be very small, the coefficient matrix $\mathbf{D}_n^o$ can advantageously be assumed constant within each sublayer, where we shall use its value at the inner radius of the jth sublayer (i.e., we take $\mathbf{D}_n^o(\eta_{j-1})$, in which $\eta_j=[\mathrm{a}_q+jh_s]/\mathrm{a}_{q+s}$; $j=1,2,\ldots,s$). Thus, within the jth sublayer, the solution to Eq. (11) can be written as

$$\mathbf{V}_n^o(\eta)=\mathbf{V}_n^o(\eta_{j-1})\exp\left[(\eta-\eta_{j-1})\mathbf{D}_n^o(\eta_{j-1})\right], \tag{12}$$

where $\left(\eta_{j-1}=[\mathrm{a}_q+(j-1)h_s]/\mathrm{a}_{q+s}\right)\leqslant\eta\leqslant\left(\eta_j=[\mathrm{a}_q+jh_s]/\mathrm{a}_{q+s}\right)$. Subsequent evaluation of Eq. (12) at the outer surface of the jth sublayer, leads to the following useful recurrence relation:

$$\mathbf{V}_n^o(\eta_j)=\mathbf{V}_n^o(\eta_{j-1})\exp\left[h_s\mathbf{D}_n^o(\eta_{j-1})/\mathrm{a}_{q+s}\right], \tag{13}$$

which relates the state variables at the outer surface of the jth sublayer to those at the inner surface. Finally, by invoking the continuity conditions between all interface layers, the state variables at the outer radius of the orthotropic layer (i.e., at $r=\mathrm{a}_{q+s}$ for which $\eta_{q+s}=\mathrm{a}_{q+s}/\mathrm{a}_{q+s}=1$) are advantageously related to those at the

inner radius (i.e., at $r = a_q$ for which $\eta_q = a_q/a_{q+s}$) via a 6×6 local modal transfer matrix $\mathbf{T}_n^o$, by

$$\mathbf{V}_n^o(\eta_{q+s}) = \mathbf{T}_n^o \mathbf{V}_n^o(\eta_q), \tag{14}$$

where $\mathbf{T}_n^o = \prod_{j=1}^{s} \exp\left[h_s \mathbf{D}_n^o(\eta_{j-1})/a_{q+s}\right]$.

2.3. Modal transfer matrix for the piezoelectric layer

A similar set of equations can be derived for the piezoelectric layer. Accordingly, the generalized constitutive relations for an axially polarized homogeneous piezoelectric cylindrical layer may be written as [23]

$$\begin{Bmatrix} \Sigma_{rr} \\ \Sigma_{\theta\theta} \\ \Sigma_{zz} \\ \Sigma_{\theta z} \\ \Sigma_{rz} \\ \Sigma_{r\theta} \end{Bmatrix} = \begin{bmatrix} c_{11}^p & c_{12}^p & c_{13}^p & 0 & 0 & 0 \\ c_{12}^p & c_{22}^p & c_{23}^p & 0 & 0 & 0 \\ c_{13}^p & c_{23}^p & c_{33}^p & 0 & 0 & 0 \\ 0 & 0 & 0 & c_{44}^p & 0 & 0 \\ 0 & 0 & 0 & 0 & c_{55}^p & 0 \\ 0 & 0 & 0 & 0 & 0 & c_{66}^p \end{bmatrix} \begin{Bmatrix} \Gamma_{rr} \\ \Gamma_{\theta\theta} \\ \Gamma_{zz} \\ 2\Gamma_{\theta z} \\ 2\Gamma_{rz} \\ 2\Gamma_{r\theta} \end{Bmatrix} - \begin{bmatrix} 0 & 0 & e_{31} \\ 0 & 0 & e_{32} \\ 0 & 0 & e_{33} \\ 0 & e_{24} & 0 \\ e_{15} & 0 & 0 \\ 0 & 0 & 0 \end{bmatrix} \begin{Bmatrix} E_r \\ E_\theta \\ E_z \end{Bmatrix}, \tag{15}$$

where Σ_{ij} and Γ_{ij} are the stress and strain components, respectively, $E_r = \partial\phi/\partial r$, $E_\theta = \partial\phi/r\partial\theta$, and $E_z = \partial\phi/\partial z$, are the electric intensity in the r, θ and z directions, respectively, ϕ is the electric potential, c_{ij}^p, e_{ij} are the elastic and piezoelectric constants, respectively, and the strain components are related to the material displacement components in the r, θ and z directions by

$$\begin{aligned} &\Gamma_{rr} = \frac{\partial U_r}{\partial r}, \quad \Gamma_{\theta\theta} = \frac{\partial U_\theta}{r\partial\theta} + \frac{U_r}{r}, \quad \Gamma_{zz} = \frac{\partial U_z}{\partial z}, \quad \Gamma_{r\theta} = \frac{1}{2}\left(\frac{\partial U_r}{r\partial\theta} + \frac{\partial U_\theta}{\partial r} - \frac{U_\theta}{r}\right), \\ &\Gamma_{\theta z} = \frac{1}{2}\left(\frac{\partial U_z}{r\partial\theta} + \frac{\partial U_\theta}{\partial z}\right), \quad \Gamma_{rz} = \frac{1}{2}\left(\frac{\partial U_z}{\partial r} + \frac{\partial U_r}{\partial z}\right), \end{aligned} \tag{16}$$

Furthermore, the equations of motion in the absence of body forces, are written as [23]

$$\begin{aligned} &\frac{\partial\Sigma_{rr}}{\partial r} + \frac{\partial\Sigma_{r\theta}}{r\partial\theta} + \frac{\partial\Sigma_{rz}}{\partial z} + \frac{1}{r}(\Sigma_{rr} - \Sigma_{r\theta}) = \rho_p \frac{\partial^2 U_r}{\partial t^2}, \quad \frac{\partial\Sigma_{r\theta}}{\partial r} + \frac{\partial\Sigma_{\theta\theta}}{r\partial\theta} + \frac{2}{r}\Sigma_{r\theta} + \frac{\partial\Sigma_{z\theta}}{\partial z} = \rho_p \frac{\partial^2 U_\theta}{\partial t^2}, \\ &\frac{\partial\Sigma_{rz}}{\partial r} + \frac{\partial\Sigma_{\theta z}}{r\partial\theta} + \frac{\Sigma_{rz}}{r} + \frac{\partial\Sigma_{zz}}{\partial z} = \rho_p \frac{\partial^2 U_z}{\partial t^2}, \quad \frac{\partial D_r}{\partial r} + \frac{\partial D_\theta}{r\partial\theta} + \frac{\partial D_z}{\partial z} + \frac{D_r}{r} = Q_f, \end{aligned} \tag{17}$$

where ρ_p is the material density of piezoelectric material, Q_f is the free charge density, and the electric displacement vector components are written as

$$\begin{aligned} D_r &= \varepsilon_{11} E_r + 2e_{15}\Gamma_{rz}, \\ D_\theta &= \varepsilon_{22} E_\theta + 2e_{24}\Gamma_{\theta z}, \\ D_z &= \varepsilon_{33} E_z + e_{31}\Gamma_{rr} + e_{32}\Gamma_{\theta\theta} + e_{33}\Gamma_{zz}, \end{aligned} \tag{18}$$

where ε_{ij} is the dielectric constant.

Now, assuming a free charge condition (i.e., $Q_f = 0$) along with the quasistatic approximation [24], we follow the state space procedure as performed for the outer orthotropic layer (see Eqs. (9)–(14)). Subsequently, we divide the piezoelectric layer into q equal sublayers ($h_q = (a_q - a_0)/q$), and ultimately invoke the continuity conditions between all interface layers. Consequently, the state variables at the outer radius of the piezoelectric layer (i.e., at $r = a_q$ for which $\eta_q = a_q/a_{q+s}$) are advantageously related to those at the inner radius (i.e., at $r = a_0$ for which $\eta_0 = a_0/a_{q+s}$) via a 8×8 local modal transfer matrix $\mathbf{T}_n^p$, by

$$\mathbf{V}_n^p(\eta_q) = \mathbf{T}_n^p \mathbf{V}_n^p(\eta_0), \tag{19}$$

where $\mathbf{V}_n^p = [U_r^n,\ U_\theta^n,\ U_z^n,\ \Sigma_{rr}^n,\ \Sigma_{r\theta}^n,\ \Sigma_{rz}^n,\ D_r^n,\ \phi_n]^{\mathrm{T}}$ is the modal state vector, $\mathbf{T}_n^p = \prod_{j=1}^{q} \exp\left[h_q \mathbf{D}_n^p(\eta_{j-1})/\mathrm{a}_{q+s}\right]$ in which $\mathbf{D}_n^p$ is a 8×8 modal coefficient matrix whose elements are given in Appendix B, and state vector $\mathbf{Y}^p$ may be expanded in terms of unknown modal coefficients as

$$Y^p = \begin{Bmatrix} U_r \\ U_\theta \\ U_z \\ \Sigma_{rr} \\ \Sigma_{r\theta} \\ \Sigma_{rz} \\ D_r \\ \phi \end{Bmatrix} = \sum_{n=0}^{\infty} \begin{Bmatrix} \mathrm{a}_{q+s} U_r^n(\eta)\cos(n\theta) \\ \mathrm{a}_{q+s} U_\theta^n(\eta)\sin(n\theta) \\ \mathrm{a}_{q+s} U_z^n(\eta)\cos(n\theta) \\ c_{44}^o \Sigma_{rr}^n(\eta)\cos(n\theta) \\ c_{44}^o \Sigma_{r\theta}^n(\eta)\sin(n\theta) \\ c_{44}^o \Sigma_{rz}^n(\eta)\cos(n\theta) \\ \sqrt{c_{44}^o \varepsilon_{33}}\, D_r^n(\eta)\cos(n\theta) \\ \mathrm{a}_{q+s}\sqrt{c_{44}^o/\varepsilon_{33}}\,\phi_n(\eta)\cos(n\theta) \end{Bmatrix} \mathrm{e}^{\mathrm{i}(k_z z-\omega t)}. \tag{20}$$

2.4. Boundary conditions and the global transfer matrix

The unknown coefficients A_n and B_n as well as the elements of the modal state variable vectors, $\mathbf{V}_n^p$ and $\mathbf{V}_n^o$, must be determined from the appropriate boundary conditions. Thus, assuming perfect bounding at the interface between the orthotropic and piezoelectric layers, continuity of normal fluid and solid velocities, continuity of the normal stress and fluid pressure, and vanishing of tangential stress at the inner/outer interface of the piezoelectric (orthotropic) layer, the following mechanical boundary conditions must be fulfilled at $r = \mathrm{a}_0,\ \mathrm{a}_{q+s}$:

$$\begin{aligned}
&(-\mathrm{i}\omega)U_r(r,\theta,\omega)\big|_{r=\mathrm{a}_0} = v_r(r,\theta,\omega)\big|_{r=\mathrm{a}_0}, && (-\mathrm{i}\omega)u_r(r,\theta,\omega)\big|_{r=\mathrm{a}_{q+s}} = v_r(r,\theta,\omega)\big|_{r=\mathrm{a}_{q+s}},\\
&\Sigma_{rr}(r,\theta,\omega)\big|_{r=\mathrm{a}_0} = -p(r,\theta,\omega)|_{r=\mathrm{a}_0}, && \sigma_{rr}(r,\theta,\omega)\big|_{r=\mathrm{a}_{q+s}} = -p(r,\theta,\omega)|_{r=\mathrm{a}_{q+s}},\\
&\Sigma_{r\theta}(r,\theta,\omega)\big|_{r=\mathrm{a}_0} = \Sigma_{rz}(r,\theta,\omega)\big|_{r=\mathrm{a}_0} = 0, && \sigma_{r\theta}(r,\theta,\omega)\big|_{r=\mathrm{a}_{q+s}} = \sigma_{rz}(r,\theta,\omega)\big|_{r=\mathrm{a}_{q+s}} = 0,\\
&\sigma_{rr}(r,\theta,\omega)\big|_{r=\mathrm{a}_q} = \Sigma_{rr}(r,\theta,\omega)\big|_{r=\mathrm{a}_q}, && \sigma_{r\theta}(r,\theta,\omega)\big|_{r=\mathrm{a}_q} = \Sigma_{r\theta}(r,\theta,\omega)\big|_{r=\mathrm{a}_q},\\
&\sigma_{rz}(r,\theta,\omega)\big|_{r=\mathrm{a}_q} = \Sigma_{rz}(r,\theta,\omega)\big|_{r=\mathrm{a}_q}, && U_r(r,\theta,\omega)\big|_{r=\mathrm{a}_q} = u_r(r,\theta,\omega)\big|_{r=\mathrm{a}_q},\\
&U_\theta(r,\theta,\omega)\big|_{r=\mathrm{a}_q} = u_\theta(r,\theta,\omega)\big|_{r=\mathrm{a}_q}, && U_z(r,\theta,\omega)\big|_{r=\mathrm{a}_q} = u_z(r,\theta,\omega)\big|_{r=\mathrm{a}_q}.
\end{aligned} \tag{21}$$

The direction of electric polarization is along the longitudinal z-axis of the hollow cylinder. Assuming that the electrodes are deposited on the inner and outer cylindrical surfaces of the piezoelectric layer (e.g., please see Fig. 1 in Ref. [25]), the corresponding open- or short-circuited electrical boundary conditions are written as [26]

$$\begin{aligned}
&\phi(r,\theta,z,\omega)\big|_{r=\mathrm{a}_0,\mathrm{a}_q} = 0 \quad \text{(short circuit)},\\
&D_r(r,\theta,z,\omega)\big|_{r=\mathrm{a}_0,\mathrm{a}_q} = 0 \quad \text{(open circuit)}.
\end{aligned} \tag{22}$$

For active control problems, it is necessary to use another electrical boundary condition in which the electric voltage can be used as a new input in addition to incident pressure. Accordingly, we assume a general (spatially dependent) electrical boundary condition applied across the electroded cylindrical surfaces, which may advantageously be expanded in form of a Fourier series as [27]

$$\begin{aligned}
&\phi(r,\theta,z,\omega)\big|_{r=\mathrm{a}_0} = 0,\\
&\phi(r,\theta,z,\omega)\big|_{r=\mathrm{a}_q} = \sum_{n=0}^{\infty} \mathrm{a}_{q+s}\sqrt{c_{44}^o/\varepsilon_{33}}\,\phi_n \cos(n\theta)\,\mathrm{e}^{\mathrm{i}(k_z z-\omega t)},
\end{aligned} \tag{23}$$

where $\phi_n(r = \mathrm{a}_q)$, the modal coefficient of electrical voltage (see Eq. (20)), may be prescribed.

Next, the linear (16×16) system of equations resulting from the boundary conditions (21) and (22) may considerably be reduced in size by incorporating the perfect bonding condition at the interface between orthotropic and piezoelectric layers (i.e., at $r=\mathrm{a}_q$) in our state space formulation. Accordingly, the modal state variable vector at the inner radius of the piezoelectric layer ($r=\mathrm{a}_0$) may advantageously be related to those at the outer radius of the orthotropic layer ($r=\mathrm{a}_{q+s}$), via a 6×8 global transfer matrix, $\mathbf{S}_n$, as

$$\mathbf{V}_n^o(\eta_{q+s})=\mathbf{S}_n\mathbf{V}_n^p(\eta_0), \tag{24}$$

where $\mathbf{S}_n=\mathbf{T}_n^o(:,:)\mathbf{T}_n^p(1:6,:)$. Subsequently, combining the expanded form of the above matrix relation with Eqs. (21) and (22), and making use of Eqs. (4), (5) and (23), after some manipulations, the following 7×7 coupled linear system of equations is obtained

$$\begin{bmatrix} C_{1,1}^n & C_{1,2}^n & 0 & 0 & -S_{1,2}^n & -S_{1,3}^n & -S_{1,7}^n\\ 0 & C_{2,2}^n & 1 & 0 & -S_{2,2}^n & -S_{2,3}^n & -S_{2,7}^n\\ 0 & C_{3,2}^n & 0 & 1 & -S_{3,2}^n & -S_{3,3}^n & -S_{3,7}^n\\ C_{4,1}^n & C_{4,2}^n & 0 & 0 & -S_{4,2}^n & -S_{4,3}^n & -S_{4,7}^n\\ 0 & C_{5,2}^n & 0 & 0 & -S_{5,2}^n & -S_{5,3}^n & -S_{5,7}^n\\ 0 & C_{6,2}^n & 0 & 0 & -S_{6,2}^n & -S_{6,3}^n & -S_{6,7}^n\\ 0 & C_{7,2}^n & 0 & 0 & T_{n(8,2)}^p & T_{n(8,3)}^p & T_{n(8,7)}^p \end{bmatrix} \begin{Bmatrix} A_n\\ B_n\\ u_\theta^n(\eta_{q+s})\\ u_z^n(\eta_{q+s})\\ U_\theta^n(\eta_0)\\ U_z^n(\eta_0)\\ D_r^n(\eta_0) \end{Bmatrix} = \begin{bmatrix} -(k_r/\omega\mathrm{a}_{q+s})\varphi_0\varepsilon_n\mathrm{i}^{n-1}J_n'(k_r\mathrm{a}_{q+s})\\ 0\\ 0\\ (\omega\rho_1/c_{44}^o)\varphi_0\varepsilon_n\mathrm{i}^{n+1}J_n(k_r\mathrm{a}_{q+s})\\ 0\\ 0\\ \phi_n \end{bmatrix}, \tag{25}$$

where

$$\begin{aligned} C_{l,2}^n &= -(S_{l,1}^nK_r\varepsilon_n\mathrm{i}^{n-1}/\omega\mathrm{a}_{q+s})J_n'(K_r\mathrm{a}_0)+(S_{l,4}^n\omega\rho_2\varepsilon_n\mathrm{i}^{n+1}/c_{44}^o)J_n(K_r\mathrm{a}_0),\\ C_{1,1}^n &= (k_r\varepsilon_n\mathrm{i}^{n-1}/\omega\mathrm{a}_{q+s})H_n^{(1)'}(k_r\mathrm{a}_{q+s}),\quad C_{4,1}^n=-(\omega\rho_1\varepsilon_n\mathrm{i}^{n+1}/c_{44}^o)H_n^{(1)}(k_r\mathrm{a}_{q+s}),\\ C_{7,2}^n &= (T_{n(8,1)}^pK_r\varepsilon_n\mathrm{i}^{n-1}/\omega\mathrm{a}_{q+s})J_n'(K_r\mathrm{a}_0)-(T_{n(8,4)}^p\omega\rho_2\varepsilon_n\mathrm{i}^{n+1}/c_{44}^o)J_n(K_r\mathrm{a}_0). \end{aligned} \tag{26}$$

where $l=1,\ldots,6$, and we note that for open circuit condition, the last row and the last column in the left-hand side matrix should be modified as $[0,\ C_{8,2}^n,\ 0,\ 0,\ T_{n(7,2)}^p,\ T_{n(7,3)}^p,\ T_{n(7,8)}^p]$ and $[-S_{1,8}^n,\ -S_{2,8}^n,\ -S_{3,8}^n,\ -S_{4,8}^n,\ -S_{5,8}^n,\ -S_{6,8}^n,\ T_{n(7,8)}^p]^{\mathrm{T}}$, respectively.

A simple look at the above linear system of Eq. (25), clearly indicates that proper selection of the modal voltage coefficient ϕ_n can cause a complete cancellation of the reflected or transmitted sound field (i.e., annihilation of the modal coefficients for the scattered or transmitted pressure: A_n or $B_n=0$). Consequently, for complete cancellation or control of the scattered sound field, the linear system (25) may advantageously be rearranged in the form:

$$\begin{bmatrix} 0 & C_{1,2}^n & 0 & 0 & -S_{1,2}^n & -S_{1,3}^n & -S_{1,7}^n\\ 0 & C_{2,2}^n & 1 & 0 & -S_{2,2}^n & -S_{2,3}^n & -S_{2,7}^n\\ 0 & C_{3,2}^n & 0 & 1 & -S_{3,2}^n & -S_{3,3}^n & -S_{3,7}^n\\ 0 & C_{4,2}^n & 0 & 0 & -S_{4,2}^n & -S_{4,3}^n & -S_{4,7}^n\\ 0 & C_{5,2}^n & 0 & 0 & -S_{5,2}^n & -S_{5,3}^n & -S_{5,7}^n\\ 0 & C_{6,2}^n & 0 & 0 & -S_{6,2}^n & -S_{6,3}^n & -S_{6,7}^n\\ -1 & C_{7,2}^n & 0 & 0 & T_{n(8,2)}^p & T_{n(8,3)}^p & T_{n(8,7)}^p \end{bmatrix} \begin{Bmatrix} \phi_n\\ B_n\\ u_\theta^n(\eta_{q+s})\\ u_z^n(\eta_{q+s})\\ U_\theta^n(\eta_0)\\ U_z^n(\eta_0)\\ D_r^n(\eta_0) \end{Bmatrix} = \begin{bmatrix} -(k_r/\omega\mathrm{a}_{q+s})\varphi_0\varepsilon_n\mathrm{i}^{n-1}J_n'(k_r\mathrm{a}_{q+s})-C_{1,1}^nA_n\\ 0\\ 0\\ (\omega\rho_1/c_{44}^o)\varphi_0\varepsilon_n\mathrm{i}^{n+1}J_n(k_r\mathrm{a}_{q+s})-C_{4,1}^nA_n\\ 0\\ 0\\ 0 \end{bmatrix}, \tag{27}$$

where ϕ_n is the modal electrical voltage coefficient required for prescription or complete annihilation of A_n. Similarly, for complete cancellation or control of the transmitted sound field, the linear system (25) may

advantageously be written in the form:

$$\begin{bmatrix} 0 & C^n_{1,1} & 0 & 0 & -S^n_{1,2} & -S^n_{1,3} & -S^n_{1,7} \\ 0 & C^n_{2,1} & 1 & 0 & -S^n_{2,2} & -S^n_{2,3} & -S^n_{2,7} \\ 0 & C^n_{3,1} & 0 & 1 & -S^n_{3,2} & -S^n_{3,3} & -S^n_{3,7} \\ 0 & C^n_{4,1} & 0 & 0 & -S^n_{4,2} & -S^n_{4,3} & -S^n_{4,7} \\ 0 & C^n_{5,1} & 0 & 0 & -S^n_{5,2} & -S^n_{5,3} & -S^n_{5,7} \\ 0 & C^n_{6,1} & 0 & 0 & -S^n_{6,2} & -S^n_{6,3} & -S^n_{6,7} \\ -1 & C^n_{7,1} & 0 & 0 & T^p_{n(8,2)} & T^p_{n(8,3)} & T^p_{n(8,7)} \end{bmatrix} \begin{Bmatrix} \phi_n \\ A_n \\ u^n_\theta(\eta_{q+s}) \\ u^n_z(\eta_{q+s}) \\ U^n_\theta(\eta_0) \\ U^n_z(\eta_0) \\ D^n_r(\eta_0) \end{Bmatrix} = \begin{bmatrix} -(k_r/\omega a_{q+s})\varphi_0\varepsilon_n i^{n-1}J'_n(k_r a_{q+s}) - C^n_{1,2}B_n \\ -C^n_{2,2}B_n \\ -C^n_{3,2}B_n \\ (\omega\rho_1/c^o_{44})\varphi_0\varepsilon_n i^{n+1}J_n(k_r a_{q+s}) - C^n_{4,2}B_n \\ -C^n_{5,2}B_n \\ -C^n_{6,2}B_n \\ -C^n_{7,2}B_n \end{bmatrix}, \tag{28}$$

where ϕ_n is the modal electrical voltage coefficient required for prescription or complete annihilation of B_n Lastly, it is noted that an optimal control strategy should be adopted for simultaneous control of both scattered and transmitted sound fields.

2.5. The global and resonance scattering coefficients

The most relevant field quantities associated with acoustic resonance scattering are the global and resonance scattering coefficients. The global scattering coefficient may be obtained from the standard definition of the backscattering form-function amplitude, which is written as [18]

$$|f_\infty(\theta=\pi,\omega)| \approx \lim_{r\to\infty}\sqrt{\frac{2r}{a_{q+s}}}\left|\frac{\varphi_1(r,\theta=\pi,\omega)}{\varphi_{\text{inc}}}\right| = \left|\sum_{n=0}^{\infty} f_n(\theta=\pi,ka_{q+s})\right|, \tag{29}$$

where the global scattering coefficient for the nth mode is given as

$$f_n(\theta,ka_{q+s}) = \frac{2\varepsilon_n}{\sqrt{\pi i k a_{q+s}}}A_n\cos(n\theta). \tag{30}$$

To extract resonance scattering coefficients from the global scattering coefficients, the non-resonance contribution which is called the background of the scatterer, has to be known. The non-resonance contributions can be in general approximated with a relevant impenetrable scatterer (e.g., hard and soft scatterers for thick and very thin shells). The rigid background is suitable for isolating the resonances of a very dense (heavy) cylinder, while the soft background has proved useful in extracting the resonances of a low density cylinder. Clearly, when densities of the solid and fluid mediums are of the same order of magnitude, neither rigid nor soft backgrounds are applicable. In cases where the impedance ratio is close to unity, the proper background behaves intermediately between the rigid and soft backgrounds. Several models have been proposed especially for the shells that can neither be considered thick nor thin and that the above backgrounds are not applicable [28–33]. Recently exact backgrounds of cylindrical shells have been found based on the absorbing scatterer, in which the elastic waves fade out quickly without forming resonances while the inertial interaction of the shell with the surrounding fluid is taken into account [28,29]. Based on this approach, the pure resonances in the scattering amplitudes of the nth normal mode can be isolated by subtracting the inherent backgrounds from the global form function as follows [29]:

$$\left|f^{(\text{res})}_n(\theta=\pi,ka_{q+s})\right| = \left|f_n(\theta=\pi,ka_{q+s}) - f^{(b)}_n(\theta=\pi,ka_{q+s})\right|, \tag{31}$$

where the inherent background coefficients are defined as

$$f^{(b)}_n(\theta,ka_{q+s}) = \frac{2\varepsilon_n}{\sqrt{\pi i k a_{q+s}}}A^{(b)}_n\cos(n\theta), \tag{32}$$

here the background scattering coefficient, $A_n^{(b)}$, which is determined by solving the problem of interaction of a plane acoustic wave with an analogous bilaminate fluid shell structure, is defined as [29,34]

$$A_n^{(b)} = (-1)\frac{k_r a_{q+s} J_n'(k_r a_{q+s}) - [F_n(0^+)]_2 J_n(k_r a_{q+s})}{k_r a_{q+s} H_n^{(1)'}(k_r a_{q+s}) - [F_n(0^+)]_2 H_n^{(1)}(k_r a_{q+s})}, \tag{33}$$

where $[F_n(0^+)]_2$ is the zero limit of the accelerance function associated with the outer layer of the bilaminate shell structure that, for the $n=0$ mode, can be obtained through the following relation [29,34,35]:

$$[F_0(0^+)]_2 = \frac{\rho_1}{\rho_o}\frac{[F_0(0^+)]_1}{\left[1 - \ln(1 - h_2/a_{q+s})[F_0(0^+)]_1\right]}, \tag{34}$$

where

$$[F_0(0^+)]_1 = \frac{\rho_o}{\rho_p}\frac{[F_0(0^+)]_0}{\left[1 - \ln(1 - h_2/a_{q+s})[F_0(0^+)]_0\right]}, \quad [F_0(0^+)]_0 = \frac{4\rho_p}{\rho_2 - 4\rho_p \ln(1 - h_1/a_{q+s})},$$

in which $h_1 = (a_q - a_0)$ and $h_2 = (a_{q+s} - a_q)$ are the thicknesses of piezoelectric and orthotropic layers, respectively. Similarly for the $n \geqslant 1$ modes, we have

$$[F_n(0^+)]_2 = \frac{\rho_1}{\rho_o}\frac{n^2 + l_2[F_n(0^+)]_1}{l_2 + [F_n(0^+)]_1}, \tag{35}$$

where

$$[F_n(0^+)]_1 = \frac{\rho_o}{\rho_p}\frac{n^2 + l_1[F_n(0^+)]_0}{l_1 + [F_n(0^+)]_0}, \quad [F_n(0^+)]_0 = \frac{\rho_p}{\rho_2} n,$$

and

$$l_{1,2} = n\frac{1 + (1 - h_{1,2}/a_{q+s})^{2n}}{1 - (1 - h_{1,2}/a_{q+s})^{2n}}.$$

Lastly, simple inspection of the above expressions indicates that, background scattering essentially depends on the structure geometry (thickness of each layer) in addition to the inertia (densities) of constituent materials and ambient fluids, i.e., it is independent of fluid compressibility and structure's elastic properties. This completes the necessary background required for the exact analysis of the problem.

3. Numerical results

In this section, we consider some numerical examples. Realizing the large number of parameters involved here while keeping in view our computing hardware limitations, we confine our attention to a particular problem. The surrounding and filling fluids are, respectively, assumed to be water and air at atmospheric pressure and ambient temperature with their physical properties as given in Table 1. The outer radius and the total thickness of the bilaminate hollow cylinder are supposed to be fixed ($a_{q+s} = 1\,\text{m}$, $h = h_1 + h_2 = 0.04\,\text{m}$). The outer layer is assumed to be fabricated from isotropic stainless steel with two independent elastic constants, while the inner piezoelectric layer is supposed to be made of PZT4 (see Table 1). A MATLAB code was constructed for computing the global modal transfer matrix ($\mathbf{S}_n$), treating the linear systems of Eqs. (25), (27) and (28), calculating the unknown scattering or transmission coefficients (A_n, B_n) as well as the corresponding electrical voltage coefficients (ϕ_n), and ultimately finding the global scattering coefficient (f_n), along with the inherent background and resonance scattering coefficients ($f_n^{(b)}, f_n^{(\text{res})}$) as a function of the non-dimensional frequency ka_{q+s} for a unit amplitude incident plane wave ($\varphi_0 = 1$). The computations were

Table 1
Physical properties of the fluid and solid mediums

Water	Steel	PZT4	
$\rho_1 = 1000$		$\rho_p = 7500$	
$c_1 = 1480$	$\rho_o = 7850$	$c_{11}^p = c_{22}^p = 139.0$,	$c_{33}^p = 115.0$
	$c_{11}^o = c_{22}^o = c_{33}^o = 282.7$	$c_{44}^p = c_{55}^p = 25.6$,	$c_{66}^p = 30.5$
	$c_{44}^o = c_{55}^o = c_{66}^o = 80.8$	$c_{13}^p = c_{23}^p = 74.0$,	$c_{12}^p = 78.1$
	$c_{12}^o = c_{13}^o = c_{23}^o = 121.1$	$\varepsilon_{11} = \varepsilon_{22} = 650$,	$\varepsilon_{33} = 560$
		$e_{31} = e_{32} = -5.2$,	$e_{15} = e_{24} = 12.7$,
		$e_{33} = 15.1$	
Air			
$\rho_2 = 1.2$			
$c_2 = 340$			

Units: $c_{ij}^{p,o}$ (GPa); $\rho_{1,2,p,o}$ (kg/m^3); ε_{ij}(10^{-11} F/m); e_{ij} (C/m^2); $c_{1,2}$ (m/s).

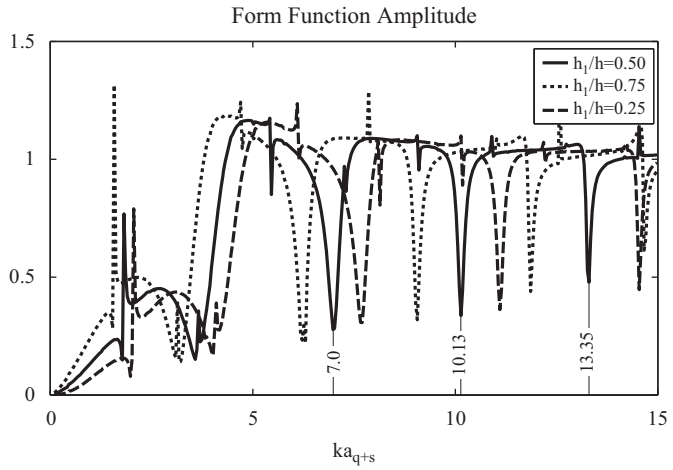

Fig. 2. The total form function spectra for a unit amplitude plane sound wave incident upon the bilaminate shell ($\alpha = 5^\circ$) for selected piezoelectric layer thickness parameters with open circuit boundary condition.

performed on a Pentium IV personal computer with a maximum number of $q_{\max}$, $s_{\max} = 100$ sublayers, and a maximum truncation constant of $n_{\max} = 150$, especially selected to assure convergence in case of a thick bilaminate hollow cylinder and also in the high-frequency range. The convergence of numerical solutions are secured in a simple trial and error manner, by increasing the number of sublayers as well as the truncation constant (i.e., by including more modes in all summations) while looking for steadiness or stability in the numerical values of the solutions. The question of convergence in acoustic scattering/radiation problems is more systematically treated, for example, in the recent works by Hasheminejad and Maleki [36], and also Hasheminejad and Azarpeyvand [37] (please see Fig. 6 in [36] for the effect of increasing number of sublayers, and Fig. 13 in [37] for the effect of increasing the truncation constant on the convergence of solutions in various frequency regimes).

Fig. 2 displays the total form function spectra for a unit amplitude plane sound wave incident upon the bilaminate hollow cylinder ($\alpha = 5^\circ$) for selected piezoelectric layer thickness parameters ($h_1/h = 0.25, 0.5, 0.75$) with open circuit boundary condition ($D_r|_{r=a_0,a_q} = 0$). Before making our general observations, we first note that for any submerged shell structure, the form function amplitude curves consists of a resonance spectra superimposed on a smooth background [18]. The resonance modes in the spectrum are primarily linked to the

standing surface waves which are formed around the cylindrical shell. Furthermore, the rigorous research works on sound wave scattering by (RST analysis of) thin shells made by several investigators [29], suggest that the relatively deep drops observed in the form function amplitude curves in our frequency range of interest in Fig. 2 may be linked to the Lamb-type waves while the sharp spikes may be related to the waves of guided type in addition to the internal fluid resonance effects [38]. More careful examination of the figure indicates that the change in the piezoelectric layer thickness has noticeable effects on both frequency and quality (amplitude and width) of the resonances (i.e., both dips and peaks in the resonance spectra). The resonances located at higher frequencies show a higher sensitivity to the change in the thickness ratio. In particular, decreasing (increasing) the thickness of the relatively stiffer steel casing, which decreases (increases) the overall stiffness of the bilaminate hollow cylinder, causes leftward (rightward) shifts in the resonance dips and spikes appearing in the backscattered spectra. It is known that such leftward or rightward shifts are consistent with the dependence of phase velocities of surface waves corresponding to these resonances [38]. This trend of shifts observed in the resonances of the bilaminate hollow cylinder may be related to the fact that in our selected range of frequency, the wavelengths of standing waves corresponding to these resonances are so considerably longer than the total thickness of the bilaminate hollow cylinder that one may expect the waves in the structure to form more or less like waves in a homogeneous single-layer equivalent shell (i.e., a shell having properties that are some kind of average of the properties of the bilaminate shell). The former statement may be verified as follows. For an obliquely incident wave upon the cylindrical structure, $\lambda_n^t = \lambda_n/\cos\beta$ is known as the projection of the total helical wavelength (λ_n) in the transverse $r\theta$-plane, where β is the wave refraction angle [18]. Knowing that a resonance indicates a standing wave pattern, an integral number (n) of the transversal component of wavelengths may be fitted around the circumference of the resonating cylindrical structure such that $\lambda_n^t = 2\pi a_{q+s}/n$ [18]. In our particular problem (i.e., for $a_{q+s} = 1$ m, $h = 0.04$ m), for the resonances associated with mode numbers less than 15 (i.e., $n \leqslant 15$) and refraction angles less than the angle of incidence (i.e., $\beta \leqslant \alpha = 5^\circ$), for example, the wavelength to thickness ratio for the cylindrical structure is simply calculated to be greater than 10 (i.e., $\lambda_n/h \geqslant 10$).

Fig. 3 illustrates how the angular distribution of far-field inherent background amplitude, $|f^{(b)}| = \left|\sum_{n=0}^{\infty} f_n^{(b)}(\theta,\omega)\right|$ is subtracted from the total form function amplitude, $|f_\infty(\theta,\omega)|$, to yield the corresponding resonance scattering amplitude, $|f_\infty^{(\mathrm{res})}| = \left|\sum_{n=0}^{\infty} f_n^{(\mathrm{res})}(\theta,\omega)\right|$ for oblique ($\alpha = 5^\circ$)incidence upon the bilaminate equal thickness PZT4/steel hollow cylinder ($h_1/h = h_2/h = 0.5$) with open circuit boundary condition at selected wavenumbers $ka_{q+s} = 7$, 10.13, 13.35 corresponding to the first three large dips observed in Fig. 2. The figure clearly displays the essence and effectiveness of the presented approach based on the subtraction of the background component from the corresponding far-field form function amplitude in order to isolate and identify the resonance frequencies [18]. In particular, the number of main lobes seen in the resonance scattering directivity plots are exactly twice the mode number corresponding to each resonance frequency (i.e., twice the number of wavelengths corresponding to each standing wave which fit the perimeter of the guiding circle in the hollow cylinder [18]). It is notable that this equality is not necessarily true for the angular diagrams of the form function amplitude. This is due to the interactions of re-radiated (resonance) component of the scattered waves with the background component within the far-field form function. Nevertheless, the resonance scattering directivities exhibit a more uniform pattern than those associated with the form function amplitude, especially at higher frequencies, which greatly relieve the resonance identification process. Consequently, the wavenumbers may be selected so that the dominant resonance frequencies corresponding to various mode numbers ($n = 2$, 3, 4) of the bilaminate hollow cylinder be readily detected. Furthermore, as the selected resonance frequency increases (i.e., the resonances corresponding to higher modes), the resonance scattering amplitude decreases which this trend point out to this fact that for the resonances belong to same family, as the frequency increases, the contribution of resonance (background) component of scattered field decreases (increases).

Fig. 4 displays the modal form function, $f_n(\theta = \pi,\ ka_{q+s})$, inherent background, $f_n^{(b)}(\theta = \pi, ka_{q+s})$, and resonance scattering, $f_n^{(\mathrm{res})}(\theta = \pi, ka_{q+s})$, spectra in addition to the associated modal surface voltage coefficient, $\phi_n(r = a_q,\ ka_{q+s})$, for selected mode numbers ($n = 0,1,\ldots,5$) at oblique ($\alpha = 5^\circ$) incidence upon the bilaminate equal-thickness PZT4/steel hollow cylinder ($h_1/h = h_2/h = 0.5$) with open circuit boundary condition. First we note that the bilaminate hollow cylinder will appear "thin" to sound of long wavelength

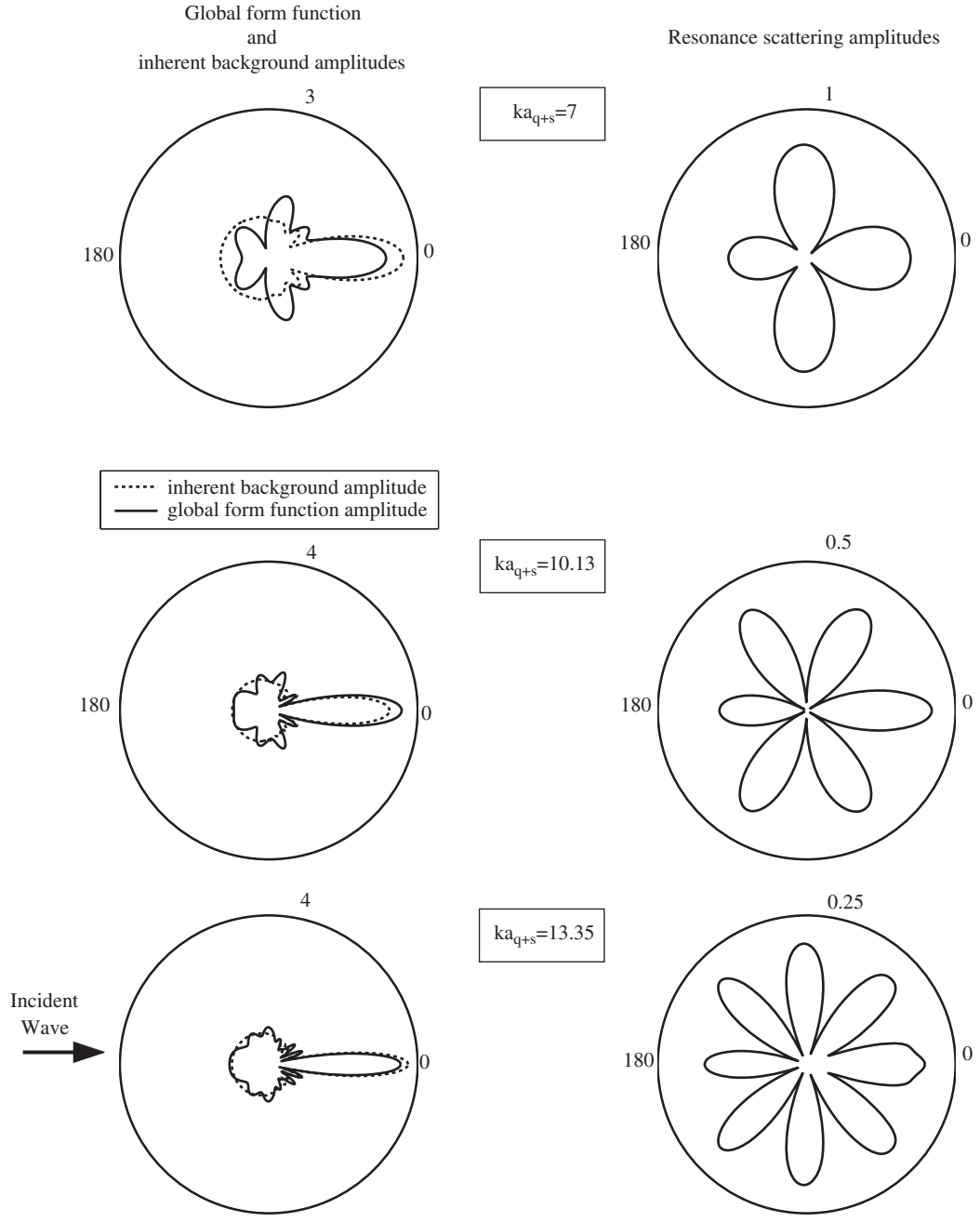

Fig. 3. Angular distribution of the far-field total form function, inherent background, and resonance scattering amplitudes for oblique ($\alpha = 5^\circ$) incidence upon the bilaminate equal thickness PZT4/steel shell ($h_1/h = h_2/h = 0.5$) with open circuit boundary condition at selected wavenumbers.

(small values of ka_{q+s}) but "thick" to sound of short wavelength (large values of ka_{q+s}) [29], the character of the background coefficients will strongly depend on the acoustic wave length in such a way that they approach the soft background amplitude for $ka_{q+s} \to 0$, and the rigid background amplitude for $ka_{q+s} \to \infty$ [29]. More specifically, at very low frequencies, the "thin" air-filled hollow cylinder behaves essentially like a cylindrical air bubble (i.e., a soft shell). Consequently, for the $n = 0$ situation (monopole mode) a notably high peak which is known in literature to be associated with the "giant monopole" resonance (i.e., analogous to air bubbles in water) is observed at a very low frequency [39]. Second, it is clear that the global scattering

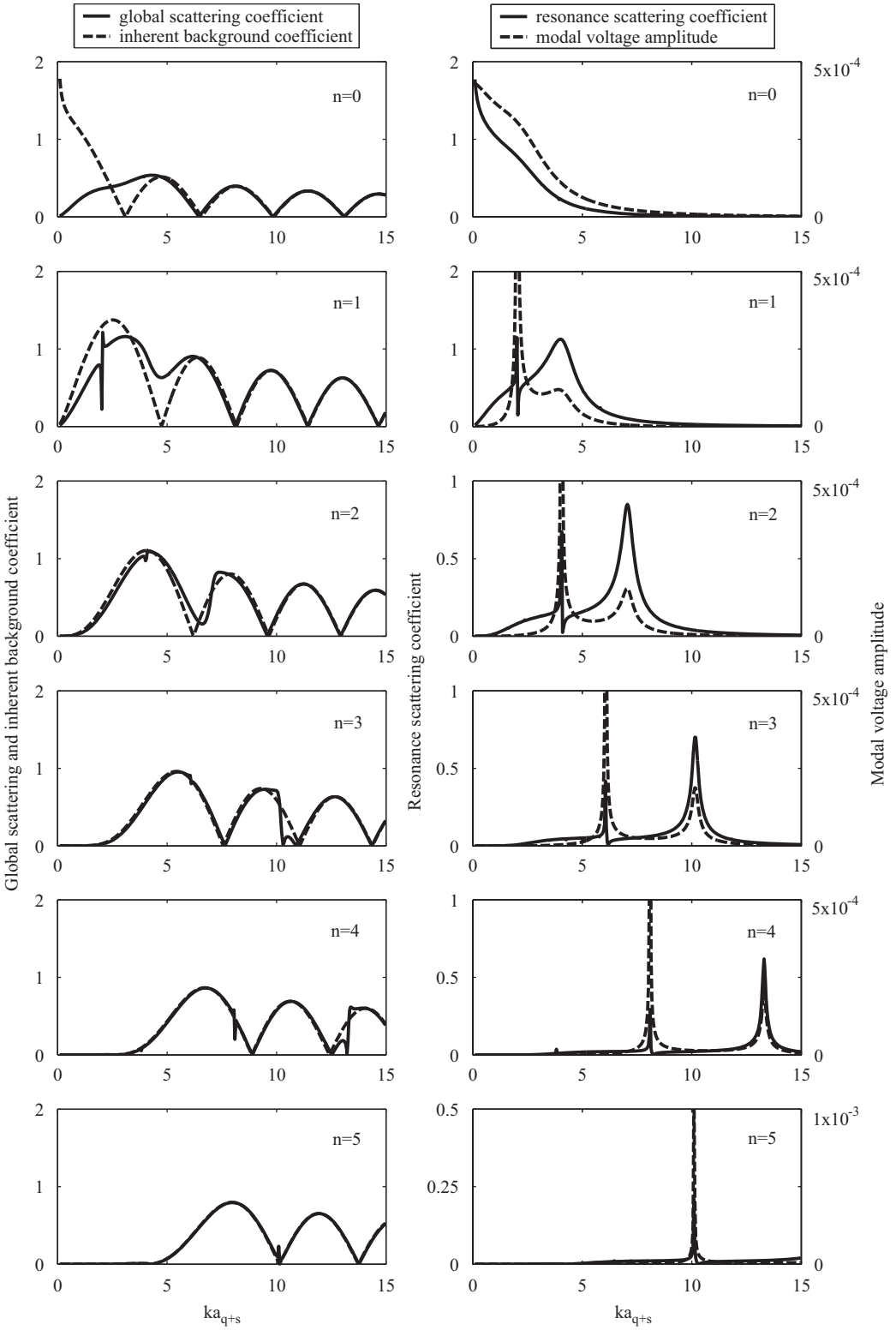

Fig. 4. The modal form function, inherent background, and resonance scattering spectra along with the associated modal surface voltage coefficient for selected mode numbers at oblique ($\alpha = 5^\circ$) incidence upon the bilaminate equal-thickness PZT4/steel shell with open circuit boundary condition.

coefficient curves (solid lines) perfectly coincide with the inherent background curves (dashed lines), except in the resonance region where the resonances are clearly isolated. As the partial wave (mode) number n increases, the locations of the dominant resonance (peak) frequencies shift toward higher wavenumbers. Furthermore, the resonance scattering coefficient plots in the right column of Fig. 4 (solid lines) confirms that the selected wavenumbers $ka_{q+s} = 7$, 10.13, 13.35 in Figs. 2 and 3, correctly correspond to the resonance frequencies associated with the $n = 2,3,4$ mode numbers, respectively. The most interesting observation is the fact that the extracted resonance frequencies, appearing in the second column plots of Fig. 4 (i.e., the resonance scattering coefficients), are exactly coincident with the resonances of the excited electrical voltage (i.e., the modal voltage amplitudes). Such good coincidence can advantageously be exploited in the use of smart (intelligent) materials in sensor design industry. Also, in the cases of $n = 1$–4 mode numbers which each of them comprises of two dominant resonance frequencies in the selected frequency range (i.e., $0 < ka_{q+s} < 15$), for the resonances with lower bandwidth, the amplitude of the excited modal voltage increases which this phenomenon implies this general fact that the resonances with lower attenuation (i.e., lower bandwidth) are more detectable than ones with greater attenuation.

Fig. 5 compares the total form function spectra for oblique ($\alpha = 5^\circ$) incidence upon the bilaminate equal-thickness PZT4/steel hollow cylinder ($h_1/h = h_2/h = 0.5$) of open circuit boundary condition $\left(D_r|_{r=a_0,a_q} = 0\right)$ with that of the closed circuit boundary condition ($\left(\phi|_{r=a_0,a_q} = 0\right)$) in a relatively wide range of frequencies ($0 < ka_{q+s} < 100$). It can be seen that, in the low-frequency range ($ka_{q+s} < 20$), the resonance frequencies corresponding to the open circuited cylinder are slightly higher than those associated with the short circuited one. In the high-frequency range ($80 < ka_{q+s} < 100$), on the other hand, the resonance frequencies for the open circuited cylinder are considerably higher than those for the short circuited hollow cylinder. This implies that we can expect a higher overall stiffness in response to the more intense electric field for the composite hollow cylinder in the open circuit electrical boundary condition. Further conclusions about the effects of the electrical boundary conditions on the mechanical behaviour of the piezoelectric hollow cylinder are very hard to make, due to the high complexity in the coupling between mechanical and electrical fields, especially in the resonance regions. Consider, for example, an axially polarized piezoelectric hollow cylinder made of PZT4 is excited by a positive axial electrical field (i.e., $E_z > 0$, E_θ, $E_r = 0$). Keeping in mind that e_{31}, $e_{32} < 0$, and $e_{33} > 0$ (see Table 1), a simple look at the constitutive Eq. (15) suggests that after imposing a positive axial electrical field ($E_z > 0$), the magnitude of axial stress component Σ_{zz} (or the effective stiffness along the axial direction) decreases, while those of the radial and transverse components Σ_{rr}, $\Sigma_{\theta\theta}$ (or the effective stiffness along radial and circumferential directions) increase, which indicates the complication of the problem.

Fig. 6 displays the total form function spectra for oblique ($\alpha = 45^\circ$) incidence upon the bilaminate equal-thickness PZT4/steel hollow cylinder ($h_1/h = h_2/h = 0.5$) with active electrical boundary conditions (Eq. (23)), where the electrical voltage, $\phi(r,\theta,\omega)|_{r=a_q} = \sum_{n=0}^{N} a_{q+s}\sqrt{c_{44}^o/\varepsilon_{33}}\phi_n \cos(n\theta)\, e^{i(k_z z-\omega t)}$, are gradually imposed (i.e., $N = 0$–8) aiming at partial cancellation or control of the reflected sound field. Also shown are the amplitude and phase of the corresponding modal voltage coefficients, ϕ_n. Here, the gradual cancellation of the backscattered sound pressure is evident as the total number of modes included in the above summation increases. In particular, the complete cancellation of the backscattered pressure in the range $0 < ka_{q+s} < 10$ is achieved by application of the first eight modal voltages ($N = 0$–8). This implies that more modes must be employed for proper acoustic cancellation at higher incident wave frequencies, where the modal voltage amplitudes themselves are also larger in overall magnitude (e.g., see the last few plots in the right column of Fig. 6). Moreover, systematic 180°phase shifts near the dominant modal amplitude dips are noted.

Fig. 7a shows the variation of normalized voltage amplitude, $\phi(r = a_q, \theta = \pi, \omega)/\left(a_{q+s}\sqrt{c_{44}^o/\varepsilon_{33}}\right)$ with angle of incidence, α, for selected piezoelectric layer thickness parameters ($h_1/h = 0.25$, 0.5, 0.75) and incident wave frequency ($ka_{q+s} = 10$). Before making our specific observations, we first note that coupling between the mechanical and electrical fields is a function of the loading characteristics (e.g., angle of incidence, incident wave frequency, etc.) in addition to the piezoelectricity ones (e.g., piezoelectric constants, e_{ij}; dielectric constants, ε_{ij}), and as a general rule, the stronger the electrical–mechanical coupling is, the less voltage is needed for successful cancellation of the reflected or transmitted pressure. Accordingly, a remarkable peak in total voltage amplitude curves, is observed at $\alpha = 0^\circ$ (normal) incidence, almost regardless the selected

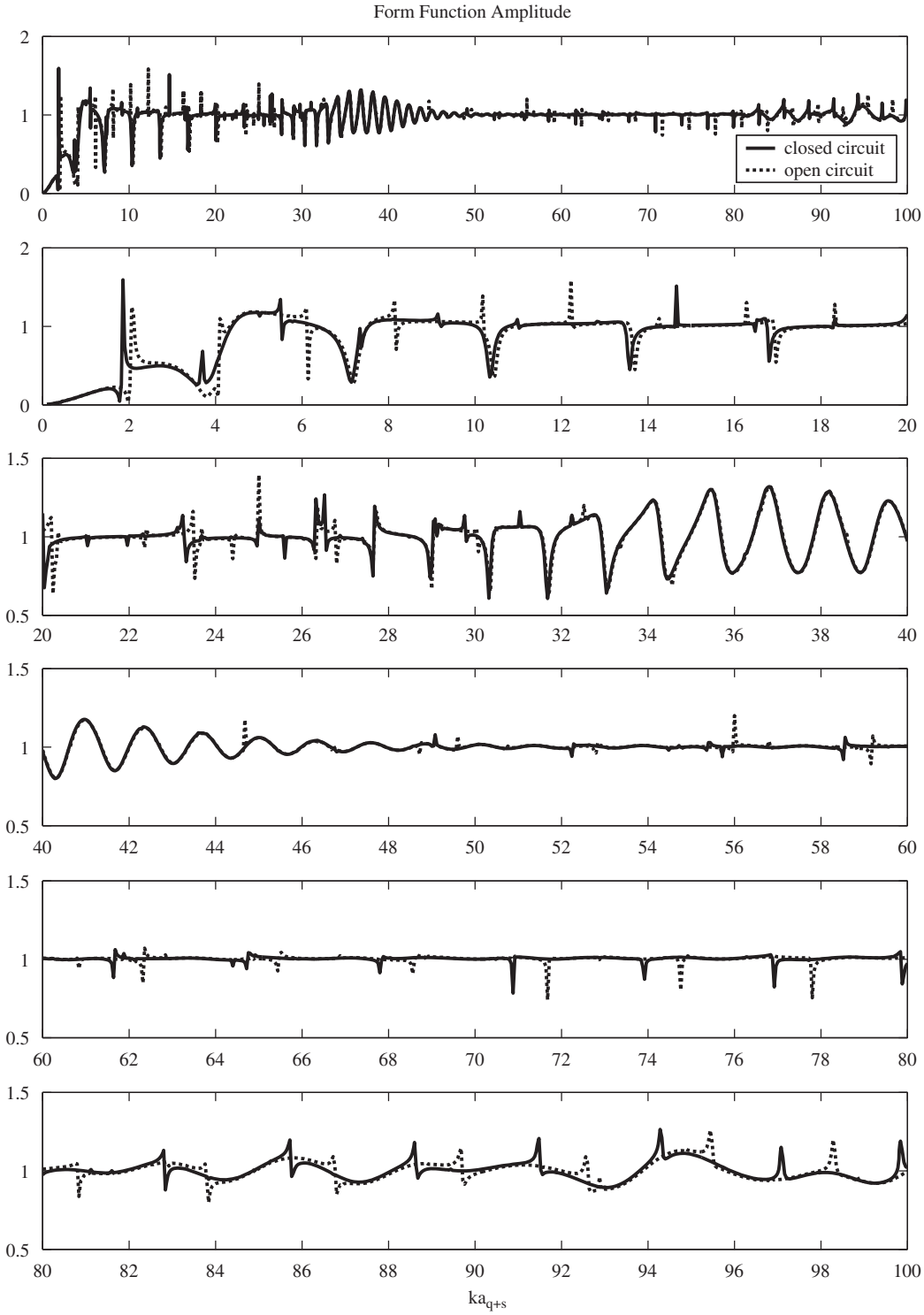

Fig. 5. The total form function spectra for oblique ($\alpha = 5^\circ$) incidence upon the bilaminate equal-thickness PZT4/steel shell with open/closed circuit boundary conditions.

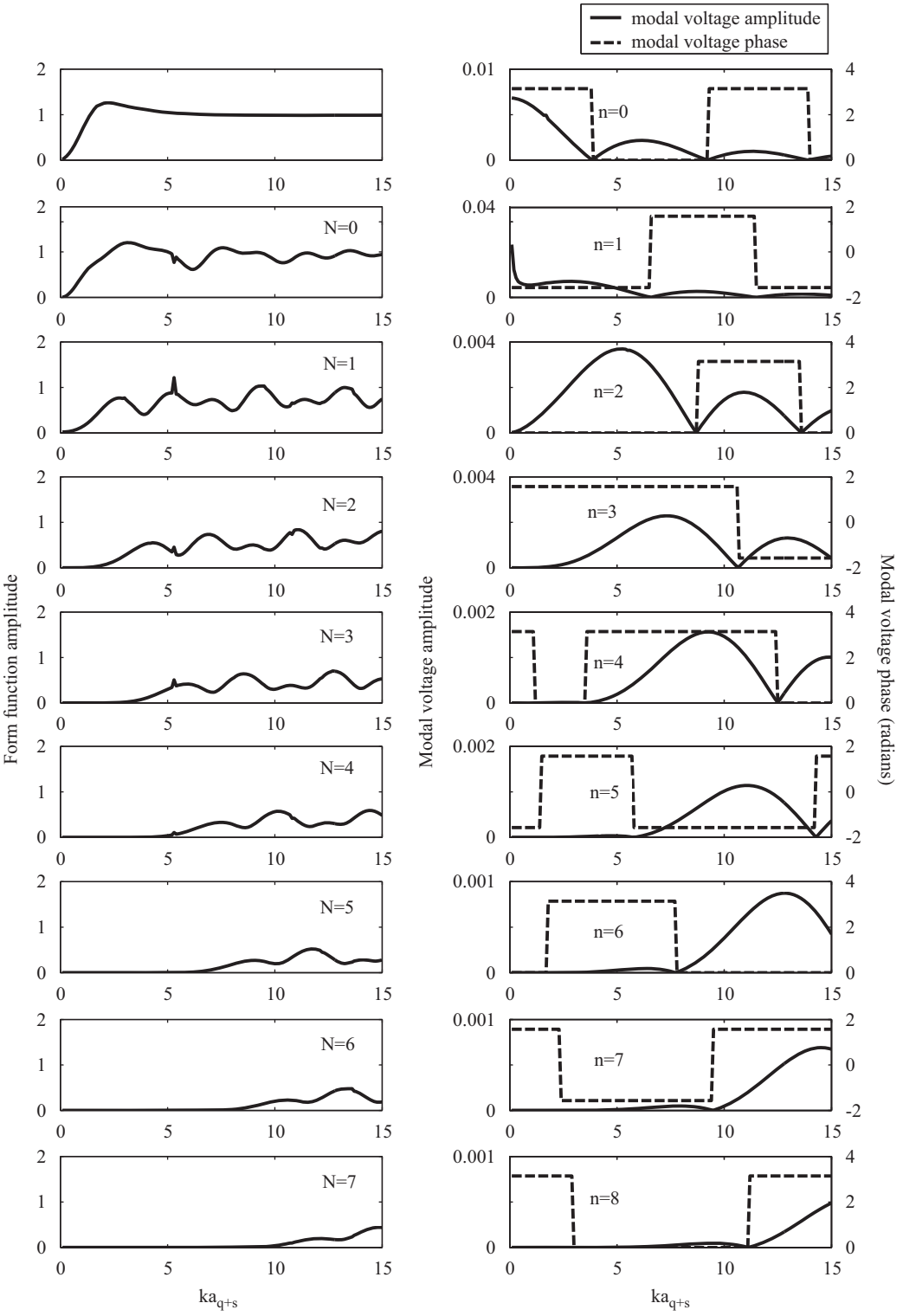

Fig. 6. The total form function spectra for oblique ($\alpha = 45°$) incidence upon the bilaminate equal-thickness PZT4/steel shell with active electrical boundary conditions for selected number of modes along with the associated modal voltage coefficients.

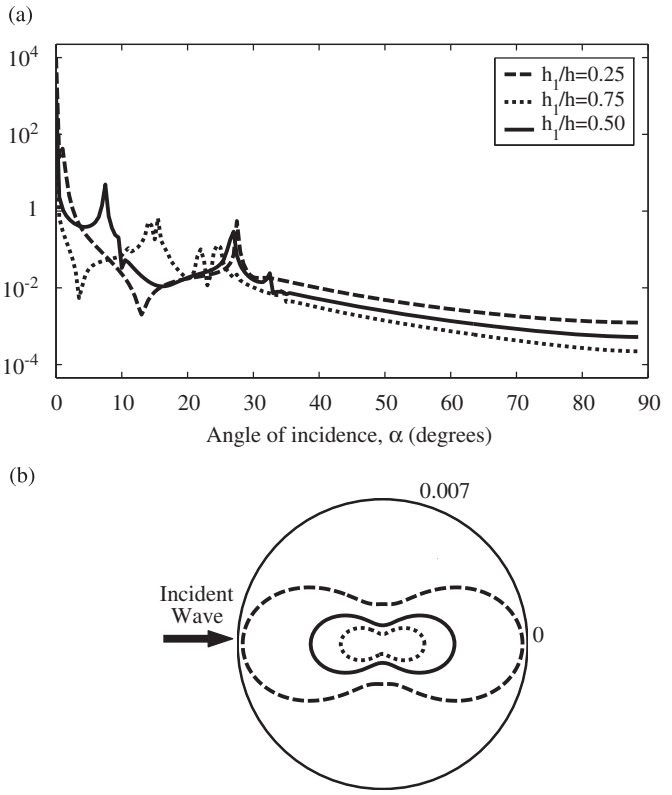

Fig. 7. (a) Variation of normalized voltage amplitude at $\theta = \pi$ with angle of incidence for selected piezoelectric layer thickness parameters and incident wave frequency ($ka_{q+s} = 10$). (b) Normalized voltage directivity pattern curves for selected angle of incidence ($\alpha = 45^\circ$), piezoelectric layer thickness parameters, and incident wave frequency ($ka_{q+s} = 10$).

incident frequency (other frequencies are not displayed for briefness) and thickness parameter. This may be linked to the fact that for this angle of incidence, the coupling between electrical and mechanical fields for an axially polarized piezoelectric layer is in weakest state that in which the axial component of the electrical field (i.e., E_z) is not excited, (i.e., $E_z = \partial\phi/\partial z \approx 0$). Consequently, this type of piezoelectric transducer is expected to be totally inefficient for near normal angles of incidence. Furthermore, for incident wave angles of about less than 35° several peaks (dips) are noted in electrical voltage amplitude curves, which imply that for this range of incidence angles, there is a weak (strong) coupling between the electrical and mechanical field of piezoelectric layer. On the other hand, for incident wave angles greater than about 35°, the required electrical voltage curves are very smooth (non-oscillatory) while they monotonically decrease in magnitude. The latter observation is due to the fact that as the incident angle increases, the level of mechanical excitement along axial direction increases, and consequently the coupling between the electrical field of axially polarized piezoelectric layer and the mechanical field of entire structure markedly amplifies. Also, the non-oscillatory behavior of the voltage may perhaps be related to fact that an increase in the incidence angle is expected to cause an increase in the refraction angle (β), for which most of the resonance frequencies move towards infinity (i.e., they cannot be easily excited) [40]. As a final observation, an inverse relationship between the thickness ratio of piezoelectric layer and the required voltage amplitude is noted in the latter range of incidence angles (i.e., greater than about 35°). The latter effect is also seen in Fig. 7b, where the corresponding normalized voltage directivity curves for selected angle of incidence ($\alpha = 45^\circ$) are displayed.

Finally, to check overall validity of the work, we first computed the variations of the global scattering as well as the associated inherent background coefficients with dimensionless frequency for the first five modes for a two-layered air-filled aluminium (Al)–tungsten carbide (WC) 2%-thickness shell submerged in water by setting $h/a_{q+s} = 0.02$, $h_1/h = 0.5$, $\rho_p = 2790\,\mathrm{kg/m^3}$, $c^p_{11} = c^p_{22} = c^p_{33} = 113.2\,\mathrm{GPa}$, $c^p_{44} = c^p_{55} = c^p_{66} = 26.8\,\mathrm{GPa}$, $c^p_{12} = c^p_{13} = c^p_{23} = 59.9\,\mathrm{GPa}$, $\rho_o = 13{,}800\,\mathrm{kg/m^3}$, $c^o_{11} = c^o_{22} = c^o_{33} = 649.2\,\mathrm{GPa}$, $c^o_{44} = c^o_{55} = c^o_{66} = 241.6\,\mathrm{GPa}$,

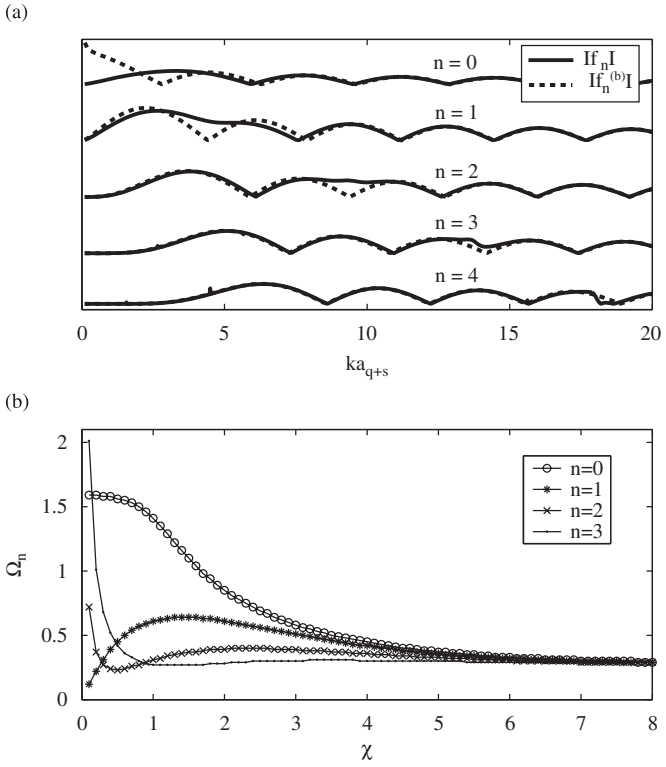

Fig. 8. (a) Variations of the global scattering and the associated inherent background coefficients with dimensionless frequency for the first five modes for a two-layered air-filled aluminium (Al)–tungsten carbide (WC) 2%-thickness cylindrical shell submerged in water. (b) Normalized eigenfrequencies, $\Omega_n = \omega \Big/ \left(k_z \sqrt{c_{44}^p/\rho_p}\right)$, as a function of dimensionless wave number, $\chi = k_z a_0$, for an evacuated axially polarized PZT4 cylindrical shell.

$c_{12}^o = c_{13}^o = c_{23}^o = 166.0\,\text{GPa}$, $\rho_1 = 1000\,\text{kg/m}^3$, $c_1 = 1480\,\text{m/s}$, $\rho_2 = 1.2\,\text{kg/m}^3$ and $c_2 = 340\,\text{m/s}$ and $e_{31} = e_{32} = e_{15} = e_{33} = e_{24} = 0\,\text{C/m}^2$ in our general MATLAB code. The outcome, as shown in Fig. 8a shows good agreement with the numerical results displayed in Fig. 11 of Ref. [29]. As a further check, we used our general formulation to determine the free vibration eigen-frequencies (the first four modes) for an evacuated thick-walled closed-circuit axially polarized PZT4 cylindrical shell. To do this we set the determinant of the left-hand side matrix in Eq. (25) equal to zero, i.e.,

$$\begin{vmatrix} C_{1,1}^n & C_{1,2}^n & 0 & 0 & -S_{1,2}^n & -S_{1,3}^n & -S_{1,7}^n \\ 0 & C_{2,2}^n & 1 & 0 & -S_{2,2}^n & -S_{2,3}^n & -S_{2,7}^n \\ 0 & C_{3,2}^n & 0 & 1 & -S_{3,2}^n & -S_{3,3}^n & -S_{3,7}^n \\ C_{4,1}^n & C_{4,2}^n & 0 & 0 & -S_{4,2}^n & -S_{4,3}^n & -S_{4,7}^n \\ 0 & C_{5,2}^n & 0 & 0 & -S_{5,2}^n & -S_{5,3}^n & -S_{5,7}^n \\ 0 & C_{6,2}^n & 0 & 0 & -S_{6,2}^n & -S_{6,3}^n & -S_{6,7}^n \\ 0 & C_{7,2}^n & 0 & 0 & T_{n(8,2)}^p & T_{n(8,3)}^p & T_{n(8,7)}^p \end{vmatrix} = 0. \tag{37}$$

Eigenequation (37) is solved numerically using the following input data: $h/a_{q+s} = 0.05$, $h_1/h \to 1$, $h_2/h \to 1$, $\rho_p = 7500\,\text{kg/m}^3$, $c_{11}^p = c_{22}^p = 139\,\text{GPa}$, $c_{33}^p = 115\,\text{GPa}$, $c_{44}^p = c_{55}^p = 25.6\,\text{GPa}$, $c_{66}^p = 30.5\,\text{GPa}$, $c_{13}^p = c_{23}^p = 74\,\text{GPa}$, $c_{12}^p = 78\,\text{GPa}$, $\varepsilon_{11} = \varepsilon_{22} = 650 \times 10^{-11}\,\text{F/m}$, $\varepsilon_{33} = 560 \times 10^{-11}\,\text{F/m}$, $e_{31} = e_{32} = -5.2\,\text{C/m}^2$, $e_{15} = e_{24} = 12.7\,\text{C/m}^2$, $e_{33} = 15.1\,\text{C/m}^2$, ρ_1, $\rho_2 \to 0\,\text{kg/m}^3$ and c_1, $c_2 \to 0\,\text{m/s}$. Fig. 8b show good agreements between the computed normalized modal frequencies, $\Omega_n = \omega \Big/ \left(k_z \sqrt{c_{44}^p/\rho_p}\right)$, as a function of dimensionless

wavenumber, $\chi = k_z a_0$, with those displayed in Fig. 1 of Ref. [23]. Here, we note that, for a given value of $0<\chi<8$, the real roots of Eq. (37) are simply obtained by searching (sweeping) for the values of Ω_n which make the real part of determinant identically zero.

4. Conclusions

The classic T-matrix method in conjunction with the state-space approach and the novel features of RST are used to present a mathematical model for acoustic wave scattering and active sound cancellation from a piezoelectric-coupled bilaminate hollow cylinder suspended in and filled with compressible ideal fluids. The numerical results reveal that the change in the piezoelectric layer thickness has noticeable effects on both location and quality of the resonances, especially in the high-frequency range. In particular, decreasing (increasing) the thickness of the stiffer steel casing causes leftward (rightward) shifts in the backscattered resonance spectra. Furthermore, the essence and effectiveness of the classic RST approach based on subtraction of the inherent background components from the corresponding far-field form function amplitudes for proper isolation and identification of the resonance frequencies of the compound structure is demonstrated. It is shown that the extracted scattering resonance frequencies are exactly coincident with the electrical voltage resonances induced in the piezoelectric layer, which is of practical value in the use of smart materials for sensor design. Also, the resonance frequencies corresponding to the open circuited piezoelectric layer are higher than those for the short circuited layer, especially in the very high-frequency range. This implies that at such high incident wave frequencies, a considerably higher overall stiffness for the open circuited composite hollow cylinder in response to the more intensely induced electric field is expected.

For the active acoustic cancellation problem, gradual extinction of the backscattered sound pressure at low to intermediate frequencies by increasing the total number of modes, which are included in the series solution, is observed. At high incident wave frequencies, considerably more modes must naturally be employed for proper acoustic cancellation. Furthermore, as the coupling between electrical and mechanical fields is in its weakest state for near normal angles of incidence, the axially polarized piezoelectric transducer is found to be totally inefficient for this angle of incidence, almost regardless of the incident wave frequency and wall thickness. Moreover, for small to moderate angles of incidence (e.g., less than about 35° for PZT4 layer) several peaks (dips) are noted in the electrical voltage amplitude curves, which imply that there is a weak (strong) coupling between the electrical field of the piezoelectric layer and the mechanical field of total structure for this range of incidence angles. For near grazing incident angles, the required electrical voltage drastically decreases, which is due to the fact that the coupling between the electrical field of axially polarized piezoelectric layer and the mechanical field of entire structure markedly increases. Also, an inverse relationship between the thickness of piezoelectric layer and the required voltage amplitude is noted for relatively large incidence angles.

Appendix A. Coefficient matrices for the orthotropic layer

$$\mathbf{M}^o = \begin{bmatrix} \mathbf{M}^o_{11} & \mathbf{M}^o_{12} \\ \mathbf{M}^o_{21} & \mathbf{M}^o_{22} \end{bmatrix},$$

where

$$\mathbf{M}^o_{11} = \begin{bmatrix} 0 & 0 & -\dfrac{\partial}{\partial z} \\ 0 & \dfrac{1}{r} & -\dfrac{\partial}{r\partial\theta} \\ -\dfrac{c^o_{13}}{c^o_{11}}\dfrac{\partial}{\partial z} & \dfrac{c^o_{12}}{c^o_{11}}\dfrac{\partial}{r\partial\theta} & -\dfrac{c^o_{12}}{c^o_{11}}\dfrac{1}{r} \end{bmatrix}, \quad \mathbf{M}^o_{12} = \begin{bmatrix} 0 & 0 & \dfrac{1}{c^o_{55}} \\ 0 & \dfrac{1}{c^o_{66}} & 0 \\ \dfrac{1}{c^o_{11}} & 0 & 0 \end{bmatrix},$$

$$\mathbf{M}_{21}^{o}=\begin{bmatrix} \dfrac{\kappa_2^o}{r}\dfrac{\partial}{\partial z} & -\dfrac{\kappa_3^o}{r^2}\dfrac{\partial}{\partial\theta} & \left(\rho_o\dfrac{\partial^2}{\partial t^2}+\dfrac{\kappa_3^o}{r^2}\right)\\ -\dfrac{(c_{44}^o+\kappa_2^o)}{r}\dfrac{\partial^2}{\partial\theta\,\partial z} & \left(\rho_o\dfrac{\partial^2}{\partial t^2}-c_{44}^o\dfrac{\partial^2}{\partial z^2}-\dfrac{\kappa_3^o}{r^2}\dfrac{\partial^2}{\partial\theta^2}\right) & -\dfrac{\kappa_3^o}{r^2}\dfrac{\partial}{\partial\theta}\\ \left(\rho_o\dfrac{\partial^2}{\partial t^2}-\kappa_1^o\dfrac{\partial^2}{\partial z^2}-\dfrac{c_{44}^o}{r^2}\dfrac{\partial^2}{\partial\theta^2}\right) & -\dfrac{(c_{44}^o+\kappa_2^o)}{r}\dfrac{\partial^2}{\partial\theta\,\partial z} & -\dfrac{\kappa_2^o}{r}\dfrac{\partial}{\partial z}\end{bmatrix},$$

$$\mathbf{M}_{22}^{o}=\begin{bmatrix} \dfrac{1}{r}\left(\dfrac{c_{12}^o}{c_{11}^o}-1\right) & -\dfrac{1}{r} & -\dfrac{\partial}{\partial z}\\ -\dfrac{c_{12}^o}{c_{11}^o}\dfrac{\partial}{r\,\partial\theta} & -\dfrac{2}{r} & 0\\ -\dfrac{c_{13}^o}{c_{11}^o}\dfrac{\partial}{\partial z} & 0 & -\dfrac{1}{r}\end{bmatrix}.$$

in which

$$\kappa_1^o=c_{33}^o-\frac{(c_{13}^o)^2}{c_{11}^o},\quad \kappa_2^o=c_{23}^o-\frac{c_{13}^o c_{12}^o}{c_{11}^o},\quad \kappa_3^o=c_{22}^o-\frac{(c_{12}^o)^2}{c_{11}^o}.$$

Also

$$\mathbf{D}_{n}^{o}=\begin{bmatrix}\mathbf{D}_{11,n}^{o} & \mathbf{D}_{12,n}^{o}\\ \mathbf{D}_{21,n}^{o} & \mathbf{D}_{22,n}^{o}\end{bmatrix},$$

where

$$\mathbf{D}_{11,n}^{o}=\begin{bmatrix} 0 & 0 & -\mathrm{i}k_z\mathrm{a}_{q+s}\\ 0 & \dfrac{1}{\eta} & \dfrac{n}{\eta}\\ -\dfrac{c_{13}^o}{c_{11}^o}\mathrm{i}k_z\mathrm{a}_{q+s} & -\dfrac{c_{12}^o n}{c_{11}^o\eta} & -\dfrac{c_{12}^o}{c_{11}^o\eta}\end{bmatrix},\quad \mathbf{D}_{12,n}^{o}=\begin{bmatrix} 0 & 0 & \dfrac{c_{44}^o}{c_{55}^o}\\ 0 & \dfrac{c_{44}^o}{c_{66}^o} & 0\\ \dfrac{c_{44}^o}{c_{11}^o} & 0 & 0\end{bmatrix},$$

$$\mathbf{D}_{21,n}^{o}=\begin{bmatrix} \dfrac{\kappa_2^o}{c_{44}^o\eta}\mathrm{i}k_z\mathrm{a}_{q+s} & \dfrac{\kappa_3^o n}{c_{44}^o\eta^2} & \dfrac{1}{c_{44}^o}\left(-\rho_o\omega^2\mathrm{a}_{q+s}^2+\dfrac{\kappa_3^o}{\eta^2}\right)\\ \dfrac{(c_{44}^o+\kappa_2^o)n}{c_{44}^o\eta}\mathrm{i}k_z\mathrm{a}_{q+s} & \dfrac{1}{c_{44}^o}\left(-\rho_o\omega^2+c_{44}^o k_z^2+\dfrac{\kappa_3^o n^2}{\eta^2}\right) & \dfrac{\kappa_3^o n}{c_{44}^o\eta^2}\\ \dfrac{1}{c_{44}^o}\left(-\rho_o\omega^2\mathrm{a}_{q+s}^2+\kappa_1^o k_z^2\mathrm{a}_{q+s}^2+\dfrac{c_{44}^o n^2}{\eta^2}\right) & -\dfrac{(c_{44}^o+\kappa_2^o)n}{c_{44}^o\eta}\mathrm{i}k_z\mathrm{a}_{q+s} & -\dfrac{\kappa_2^o}{c_{44}^o\eta}\mathrm{i}k_z\mathrm{a}_{q+s}\end{bmatrix},$$

$$\mathbf{D}_{22,n}^{o}=\begin{bmatrix} \dfrac{1}{\eta}\left(\dfrac{c_{12}^o}{c_{11}^o}-1\right) & -\dfrac{1}{\eta} & -\mathrm{i}k_z\mathrm{a}_{q+s}\\ \dfrac{c_{12}^o n}{c_{11}^o\eta} & -\dfrac{2}{\eta} & 0\\ -\dfrac{c_{13}^o}{c_{11}^o}\mathrm{i}k_z\mathrm{a}_{q+s} & 0 & -\dfrac{1}{\eta}\end{bmatrix}.$$

Appendix B. Coefficient matrices for the piezoelectric layer

$$\mathbf{M}^p = \begin{bmatrix} \mathbf{M}^p_{11} & \mathbf{M}^p_{12} \\ \mathbf{M}^p_{21} & \mathbf{M}^p_{22} \end{bmatrix},$$

where

$$\mathbf{M}^p_{11} = \begin{bmatrix} -\frac{c^p_{12}}{c^p_{11}}\frac{1}{r} & -\frac{c^p_{12}}{c^p_{11}}\frac{1}{r}\frac{\partial}{\partial\theta} & -\frac{c^p_{13}}{c^p_{11}}\frac{\partial}{\partial z} & \frac{1}{c^p_{11}} \\ -\frac{\partial}{r\,\partial\theta} & \frac{1}{r} & 0 & 0 \\ -\frac{\partial}{\partial z} & 0 & 0 & 0 \\ \rho_p\frac{\partial^2}{\partial t^2}+\frac{\kappa^p_1}{r^2} & \frac{\kappa^p_1}{r^2}\frac{\partial}{\partial\theta} & \frac{\kappa^p_2}{r}\frac{\partial}{\partial z} & \left(\frac{c^p_{12}}{c^p_{11}}-1\right)\frac{1}{r} \end{bmatrix}, \quad \mathbf{M}^p_{12} = \begin{bmatrix} 0 & 0 & 0 & \frac{e_{31}}{c^p_{11}}\frac{\partial}{\partial z} \\ \frac{1}{c^p_{66}} & 0 & 0 & 0 \\ 0 & \frac{\varepsilon_{11}}{\ell} & \frac{e_{15}}{\ell} & 0 \\ -\frac{\partial}{r\,\partial\theta} & -\frac{\partial}{\partial z} & 0 & \frac{\kappa^p_3}{r}\frac{\partial}{\partial z} \end{bmatrix},$$

$$\mathbf{M}^p_{21} = \begin{bmatrix} -\frac{\kappa^p_1}{r^2}\frac{\partial}{\partial\theta} & \rho_p\frac{\partial^2}{\partial t^2}-\frac{\kappa^p_1}{r^2}\frac{\partial^2}{\partial\theta^2}-c^p_{44}\frac{\partial^2}{\partial z^2} & -\frac{c^p_{44}+\kappa^p_2}{r}\frac{\partial^2}{\partial\theta\,\partial z} & -\frac{c^p_{12}}{c^p_{11}}\frac{\partial}{r\,\partial\theta} \\ -\frac{\kappa^p_2}{r}\frac{\partial}{\partial z} & -\frac{c^p_{44}+\kappa^p_2}{r}\frac{\partial^2}{\partial\theta\,\partial z} & \rho_p\frac{\partial^2}{\partial t^2}-\frac{c^p_{44}}{r^2}\frac{\partial^2}{\partial\theta^2}-\kappa^p_4\frac{\partial^2}{\partial z^2} & -\frac{c^p_{13}}{c^p_{11}}\frac{\partial}{\partial z} \\ -\frac{\kappa^p_3}{r}\frac{\partial}{\partial z} & -\frac{e_{24}+\kappa^p_3}{r}\frac{\partial^2}{\partial\theta\,\partial z} & \frac{e_{24}}{r^2}\frac{\partial^2}{\partial\theta^2}-\kappa^p_5\frac{\partial^2}{\partial z^2} & \frac{e_{31}}{c^p_{11}}\frac{\partial}{\partial z} \\ 0 & 0 & 0 & 0 \end{bmatrix},$$

$$\mathbf{M}^p_{22} = \begin{bmatrix} -\frac{2}{r} & 0 & 0 & -\frac{e_{24}+\kappa^p_3}{r}\frac{\partial^2}{\partial\theta\,\partial z} \\ 0 & -\frac{1}{r} & 0 & -\frac{e_{24}}{r^2}\frac{\partial^2}{\partial\theta^2}-\kappa^p_5\frac{\partial^2}{\partial z^2} \\ 0 & 0 & -\frac{1}{r} & \frac{\varepsilon_{22}}{r^2}\frac{\partial^2}{\partial\theta^2}+\kappa^p_6\frac{\partial^2}{\partial z^2} \\ 0 & \frac{e_{15}}{\ell} & -\frac{c^p_{55}}{\ell} & 0 \end{bmatrix},$$

in which $\ell = c^p_{55}\varepsilon_{11} + e^2_{15}$, and

$$\kappa^p_1 = c^p_{22} - \frac{(c^p_{12})^2}{c^p_{11}}, \quad \kappa^p_2 = c^p_{23} - \frac{c^p_{12}c^p_{13}}{c^p_{11}}, \quad \kappa^p_3 = e_{32} - \frac{c^p_{12}e_{31}}{c^p_{11}},$$
$$\kappa^p_4 = c^p_{33} - \frac{(c^p_{13})^2}{c^p_{11}}, \quad \kappa^p_5 = e_{33} - \frac{c^p_{13}e_{31}}{c^p_{11}}, \quad \kappa^p_6 = \varepsilon_{33} + \frac{e^2_{31}}{c^p_{11}}.$$

Also

$$\mathbf{D}^p = \begin{bmatrix} \mathbf{D}^p_{11} & \mathbf{D}^p_{12} \\ \mathbf{D}^p_{21} & \mathbf{D}^p_{22} \end{bmatrix},$$

where

$$\mathbf{D}_{11}^{p}=\begin{bmatrix} -\dfrac{c_{12}^{p}}{c_{11}^{p}}\dfrac{1}{\eta} & -\dfrac{c_{12}^{p}}{c_{11}^{p}}\dfrac{n}{\eta} & -\dfrac{c_{13}^{p}}{c_{11}^{p}}ik_z\mathrm{a}_{q+s} & -\dfrac{c_{44}^{o}}{c_{11}^{p}} \\ \dfrac{n}{\eta} & \dfrac{1}{\eta} & 0 & 0 \\ -ik_z\mathrm{a}_{q+s} & 0 & 0 & 0 \\ \left(-\rho_q\omega^2\mathrm{a}_{q+s}^2+\dfrac{\kappa_1^p}{\eta^2}\right)\dfrac{1}{c_{44}^{o}} & \dfrac{\kappa_1^p}{c_{44}^{o}}\left(\dfrac{1}{\eta}\right)^2 n & \dfrac{\kappa_2^p}{c_{44}^{o}}\dfrac{-ik_z\mathrm{a}_{q+s}}{\eta^2} & \left(\dfrac{c_{12}^{p}}{c_{11}^{p}}-1\right)\dfrac{1}{\eta} \end{bmatrix}$$

$$\mathbf{D}_{12}^{p}=\begin{bmatrix} 0 & 0 & 0 & -\dfrac{e_{31}}{c_{11}^{p}}\mathrm{i}k_z\mathrm{a}_{q+s}\sqrt{\dfrac{c_{44}^{o}}{\varepsilon_{33}}} \\ \dfrac{c_{44}^{o}}{c_{66}^{p}} & 0 & 0 & 0 \\ 0 & \dfrac{c_{44}^{o}\varepsilon_{11}}{\ell} & \dfrac{e_{15}}{\ell}\sqrt{c_{44}^{o}\varepsilon_{33}} & 0 \\ -\dfrac{n}{\eta} & -\mathrm{i}k_z\mathrm{a}_{q+s} & 0 & \dfrac{\kappa_3^p}{\eta}\dfrac{\mathrm{i}k_z\mathrm{a}_{q+s}}{\sqrt{c_{44}^{o}\varepsilon_{33}}} \end{bmatrix},$$

$$\mathbf{D}_{21}^{p}=\begin{bmatrix} -\dfrac{\kappa_1^p}{c_{44}^{o}}\left(\dfrac{1}{\eta}\right)^2 n & \left(-\rho_p\omega^2\mathrm{a}_{q+s}^2+\dfrac{\kappa_1^p}{\eta^2}n^2+c_{44}^{p}k_z^2\mathrm{a}_{q+s}^2\right)\dfrac{1}{c_{44}^{o}} & \dfrac{c_{44}^{p}+\kappa_2^p}{\eta}\dfrac{n\mathrm{i}k_z\mathrm{a}_{q+s}}{c_{44}^{o}} & \dfrac{c_{12}^{p}}{c_{11}^{p}}\dfrac{n}{\eta} \\ -\dfrac{\kappa_2^p\mathrm{i}k_z\mathrm{a}_{q+s}}{c_{44}^{o}\eta} & -\dfrac{c_{44}^{p}+\kappa_2^p}{\eta}\dfrac{\mathrm{i}k_z\mathrm{a}_{q+s}n}{c_{44}^{o}} & \left(-\rho_p\omega^2\mathrm{a}_{q+s}^2+\dfrac{c_{44}^{p}n^2}{\eta^2}+\kappa_4^pk_z^2\mathrm{a}_{q+s}^2\right)\dfrac{1}{c_{44}^{o}} & -\dfrac{c_{13}^{p}}{c_{11}^{p}}\mathrm{i}k_z\mathrm{a}_{q+s} \\ -\dfrac{\kappa_3^p}{\eta}\dfrac{\mathrm{i}k_z\mathrm{a}_{q+s}}{\sqrt{c_{44}^{o}\varepsilon_{33}}} & -\dfrac{e_{24}+\kappa_3^p}{\eta}\dfrac{n\mathrm{i}k_z\mathrm{a}_{q+s}}{\sqrt{c_{44}^{o}\varepsilon_{33}}} & \left(\dfrac{e_{24}}{\eta^2}n^2+\kappa_5^pk_z^2\mathrm{a}_{q+s}^2\right)\dfrac{1}{\sqrt{c_{44}^{o}\varepsilon_{33}}} & -\dfrac{e_{31}}{c_{11}^{p}}\mathrm{i}k_z\mathrm{a}_{q+s}\sqrt{\dfrac{c_{44}^{o}}{\varepsilon_{33}}} \\ 0 & 0 & 0 & 0 \end{bmatrix},$$

$$\mathbf{D}_{22}^{p}=\begin{bmatrix} -\dfrac{2}{\eta} & 0 & 0 & \dfrac{e_{24}+\kappa_3^p}{\eta}\dfrac{n\mathrm{i}k_z\mathrm{a}_{q+s}}{\sqrt{c_{44}^{o}\varepsilon_{33}}} \\ 0 & -\dfrac{1}{\eta} & 0 & \left(\dfrac{e_{24}}{\eta^2}n^2+\kappa_5^pk_z^2\mathrm{a}_{q+s}^2\right)\dfrac{1}{\sqrt{c_{44}^{o}\varepsilon_{33}}} \\ 0 & 0 & -\dfrac{1}{\eta} & \left(-\dfrac{\varepsilon_{22}}{\eta^2}n^2-\kappa_6^pk_z^2\mathrm{a}_{q+s}^2\right)\dfrac{1}{\varepsilon_{33}} \\ 0 & \dfrac{e_{15}}{\ell}\sqrt{c_{44}^{o}\varepsilon_{33}} & -\dfrac{c_{55}^{p}}{\ell}\varepsilon_{33} & 0 \end{bmatrix}.$$

References

[1] D. Berlincourt, Piezoelectric ceramics: characteristics and applications, *Journal of the Acoustical Society of America* 70 (1981) 1586–1595.
[2] O.B. Wilson, Introduction to the Theory and Design of Sonar Transducers, Peninsula, Los Altos, CA, 1988.
[3] I.J. Busch-Vishniac, *Electromechanical Sensors and Actuators*, Springer, New York, 1999.
[4] D.D. Ebenezer, K. Ravichandran, R. Ramesh, Forced responses of solid axially polarized piezoelectric ceramic finite cylinders with internal losses, *Journal of the Acoustical Society of America* 117 (2005) 3645–3656.
[5] M.C. Dokmeci, Vibrations of piezoelectric crystals, *International Journal of Engineering Science* 18 (1980) 431–448.

[6] T.R. Howarth, V.K. Varadan, X. Bao, V.V. Varadan, Piezocomposite coating for active underwater sound reduction, *Journal of the Acoustical Society of America* 91 (1992) 823–831.
[7] N.A. Shul'ga, S.I. Rudnitskii, O.B. Kachaenko, Electroacoustic sensitivity of a cylindrical piezoceramic shell in an acoustic medium, *Prikladnaya Mekhanika* 25 (1989) 44–48.
[8] S.I. Rudnitskii, N.A. Shul'ga, Directivity of a cylindrical piezoelectric shell with segmented electrodes in an acoustic medium, *International Applied Mechanics* 29 (1993) 712–716.
[9] A.E. Babaev, Y.N. Ryabukha, V.G. Savin, Interaction of an acoustic shock wave with a cylindrical piezoelectric shell located near a plane boundary, *Prikladnaya Mekhanika* 29 (1991) 46–54.
[10] M.M. Belova, M.N. Moskal'kov, V.G. Savin, Numerical solution of the problem of sound emission by a cylindrical piezoelectric vibrator excited by electric pulses, *Matematika* 61 (1987) 30–37.
[11] I.V. Vovk, V.N. Oliynik, Sound radiation by a cylindrical piezoelastic shell with an asymmetric insertion, *Journal of the Acoustical Society of America* 99 (1996) 133–138.
[12] V.E. Glazanov, A.V. Mikhailov, Sound radiation from a cylindrical transducer filled with an elastic medium, *Acoustical Physics* 50 (2004) 454–461.
[13] A.E. Babaev, A.A. Babaev, Generation of nonstationary waves by a thick-walled piezoceramic cylinder excited by electric signals, *IEEE Transactions on Ultrasonics, Ferroelectrics, and Frequency Control* 52 (2005) 518–524.
[14] Y. Zhang, Z.P. Tong, Z.Y. Zhang, H.X. Hua, Finite element modelling of a fluid-filled cylindrical shell with piezoelectric damping, *Journal of Vibration Engineering* 19 (2006) 24–30.
[15] H. Liu, J.J. Lee, Scattering of a small angle incident acoustic wave from a submerged piezoelectric cylinder, *Key Engineering Materials* 306 (2006) 1229–1234.
[16] C.L. Scandrett, Y.S. Shina, K.C. Hungb, M.S. Khanb, C.C. Lilianc, Cancellation techniques in underwater scattering of acoustic signals, *Journal of Sound and Vibration* 272 (2004) 513–537.
[17] A.D. Pierce, *Acoustics: An Introduction to its Physical Principles and Applications*, American Institute of Physics, New York, 1991.
[18] N.D. Veksler, *Resonance Acoustic Spectroscopy, Springer Series on Wave Phenomena*, Springer, Berlin, 1993.
[19] M. Abramowitz, I.A. Stegun, *Handbook of Mathematical Functions*, National Bureau of Standards, Washington, DC, 1964.
[20] M.J.P. Musgrave, Crystal Acoustics, Holden-Day Series in Mathematical Physics, 1970.
[21] J.D. Achenbach, *Wave Propagation in Elastic Solids*, North-Holland, New York, 1976.
[22] W.Q. Chen, Z.G. Bian, H.J. Ding, Three dimensional vibration analysis of fluid filled orthotropic FGM cylindrical shells, *International Journal of Mechanical Science* 46 (2004) 159–171.
[23] W.Q. Chen, Z.G. Bian, C.F. Lv, H.J. Ding, 3D free vibration analysis of a functionally graded piezoelectric hollow cylinder filled with compressible fluid, *International Journal of Solids and Structures* 41 (2004) 947–964.
[24] B.A. Auld, *Acoustic Fields and Waves in Solids*, Krieger, Malabar, FL, 1990.
[25] P. Kielczynski, W. Pajewski, M. Szalewski, Admittance of axially polarized lossy piezoceramic cylinders loaded with a viscoelastic liquid, *Journal of Applied Physics* 91 (2002) 10181–10187.
[26] N.T. Adelman, Y. Stavsky, E. Segal, Radial vibrations of axially polarized piezoelectric ceramic cylinders, *Journal of American Society of America* 57 (1976) 356–360.
[27] C. Scandrett, Scattering and active acoustic control from a submerged spherical shell, *Journal of American Society of America* 111 (2002) 893–907.
[28] M.S. Choi, Y.S. Joo, J.P. Lee, Inherent background coefficients for submerged cylindrical shells, *Journal of the Acoustical Society of America* 101 (1997) 1743–1745.
[29] Y.S. Joo, J.G. Ih, M.S. Choi, Inherent background coefficients for acoustic resonance scattering from submerged, multilayered, cylindrical structures, *Journal of the Acoustical Society of America* 103 (1998) 900–910.
[30] G.C. Gaunaurd, M.F. Werby, Acoustic resonance scattering by submerged elastic shell, *Applied Mechanics Review* 43 (1990) 171–208.
[31] M.F. Werby, G.C. Gaunaurd, Transition from soft to rigid behaviour in scattering from submerged thin elastic shells, *Acoustic Letters* 9 (1986) 89–93.
[32] G.C. Gaunaurd, Hybrid background coefficients to isolate the resonance spectrum of submerged shells, *Journal of the Acoustical Society of America* 92 (1992) 1981–1984.
[33] D.N. Veksler, Intermediate background in problems of sound waves scattering by elastic shells, *Acustica* 76 (1992) 1–9.
[34] J.Y. Kim, J.G. Ih, Scattering of plane acoustic waves by a transversely isotropic cylindrical shell-application to material characterization, *Applied Acoustics* 64 (2003) 1187–1204.
[35] M.S. Choi, Inherent background coefficient of the axisymmetric mode in acoustic resonance scattering from a system of multilayered shells, *Journal of the Korean Physical Society* 37 (2000) 519–526.
[36] S.M. Hasheminejad, M. Maleki, Interaction of a plane progressive sound wave with a functionally graded spherical shell, *Ultrasonics* 45 (2006) 165–177.
[37] S.M. Hasheminejad, M. Azarpeyvand, Energy distribution and radiation loading of a cylindrical source suspended within a nonconcentric fluid cylinder, *Acta Mechanica* 164 (2003) 15–30.
[38] S.M. Hasheminejad, M. Rajabi, Acoustic scattering characteristics of a thick-walled orthotropic cylindrical shell at oblique incidence, *Ultrasonics* 47 (2007) 32–48.
[39] J.D. Murphy, E.D. Breitenbach, H. Uberall, Resonance scattering of acoustic waves from cylindrical shells, *Journal of the Acoustical Society of America* 64 (1978) 677–683.
[40] J.M. Conoir, P. Rembert, O. Lenoir, J.L. Izbicki, Relation between surface helical waves and elastic cylinder resonances, *Journal of the Acoustical Society of America* 93 (1993) 1300–1307.